Available online at www.sciencedirect.com
ScienceDirect
Journal of Sound and Vibration 303 (2007) 1–28
JOURNAL OF SOUND AND VIBRATION
www.elsevier.com/locate/jsvi

Dynamics of a Jeffcott rotor with slant crack

Ashish K. Darpe

Department of Mechanical Engineering, Indian Institute of Technology, Delhi-110016, India

Received 23 May 2005; received in revised form 1 March 2006; accepted 22 July 2006
Available online 13 March 2007

Abstract

A simple Jeffcott rotor model of a rotor with a slant crack is presented. Flexibility matrix of the rotor with slant crack is developed and the stiffness coefficients based on the flexibility values are used in the equations of motion. Response-dependent nonlinear breathing crack model is used to evaluate unbalance response of the cracked rotor. Comparison between rotor with slant and transverse crack is made with regard to the flexibility/stiffness coefficients and the unbalance response characteristics. The flexibility matrix for slant crack case is more populated with additional cross-coupled coefficients compared to the transverse crack case. The rotor with slant crack is found to be stiffer in lateral and longitudinal directions, but more flexible in torsion, compared to the one with transverse crack. The response of the rotor with the two types of cracks (transverse and slant) is analysed at subharmonic resonances to explore possibilities of distinctive features in their response. Spectrum cascade plot for lateral and longitudinal vibrations exhibit distinctive response features for slant and transverse crack rotors.

1. Introduction

An ever-increasing quest for more power has led to severely stressed rotors, particularly in power generation sector. With several locations where stresses (both mechanical and thermal) can increase despite best design practices, fatigue cracks are always a possibility in such rotors. If undetected early, such cracks can pose a potential source of catastrophic failures. Several researchers have therefore conducted extensive investigations on the response of cracked rotor over the last three decades. An in depth literature review of dynamics of cracked rotors was published by Wauer [1] and later a more exhaustive state of the art review on rotors as well as structures was published by Dimarogonas [2]. Recently, Sabnavis et al. [3] have reviewed the literature on cracked shaft detection and diagnosis that appeared after 1990, grouping the literature under vibration-based methods, modal testing and non-traditional methods. Gupta [4] reviewed various diagnostic strategies for transverse crack in rotor shaft and blades and discussed their limitations and advantages in order to evolve effective crack detection techniques. He also outlined improvements to enhance applicability of these strategies to real systems.

According to Bently [5], changes in the synchronous ($1x$) amplitude and phase, difficulty in trim balancing and in particular, insensitivity of the $2x$ component to balancing are the most important indicators of the shaft

E-mail address: akdarpe@mech.iitd.ernet.in.

0022-460X/$ - see front matter © 2007 Elsevier Ltd. All rights reserved.
doi:10.1016/j.jsv.2006.07.052

Nomenclature

a	depth of the crack
c	damping coefficient
CCLP	crack closure line position
D	diameter of the shaft
e	dimensionless eccentricity of the unbalance (ε/δ)
E	modulus of elasticity
g_{ij}	flexibility coefficient of the cracked rotor, where $i, j = 1,\ldots,6$
k_{ij}	stiffness coefficient $i = \xi,\eta,y,z,u$ $j = \xi,\eta, y,z,u$
m	mass of the disc
P_i	force acting on crack cross-section of the shaft in ith direction
r	dimensionless speed of rotation ($r = \omega/\omega_0$)
R	radius of the shaft
y,z,u	rotor response in vertical, horizontal and axial direction, respectively
y-z-u	stationary coordinate system
$\bar{a}$	crack depth ratio (a/D)
$\bar{y}, \bar{z}, \bar{u}$	dimensionless rotor response in vertical, horizontal and axial direction, respectively
K_i^j	stress intensity factor for mode j due to force along ith direction
α	depth of crack at any distance χ_0
ω	rotational speed
θ	angle of orientation of slant crack relative to axis of the shaft
ε	eccentricity of centre of mass at the disc location
β	orientation of unbalance relative to the crack direction (ξ)
υ	Poisson's ratio
δ	static deflection of the uncracked rotor
$\varphi(t)$	angle of rotation
ξ–η–u	rotor fixed coordinate system
ω_0	bending natural frequency of the uncracked rotor
χ_0	distance measured from centre of shaft along the crack edge (direction 2′)
σ_i^θ, τ_i^θ	normal and shear stress components along ith direction ($i = 1$–6) in crack cross-section (coordinate system 1′–2′–3′)
σ_i, τ_i	normal and shear stress components along ith direction ($i = 1$–6) in transverse plane (coordinate system 1–2–3)

crack. He also emphasized on the measurement of the slow roll bow vector and the use of polar plot for crack monitoring. The $2x$ component also grows due to the induced asymmetry. Bently and Werner [6] discussed design principles to avoid occurrence of rotor crack and stressed the need to monitor phase of vibration as changes in phase could be observed months before the vibration amplitude and frequency changed.

While several authors [7–9] mainly focussed their work on unbalance lateral vibration response of the cracked rotor, others [10–14] investigated and proposed new methods of crack detection based on coupling of vibration due to the presence of crack in a rotor after Papadopoulos and Dimarogonas [15] introduced the coupling phenomenon in rotors. Collins et al. [11] and Darpe et al. [12,13] studied the detection of cracks using axial impulses to a rotating cracked shaft. They reported the presence of combination harmonics in the lateral vibration spectrum. Gounaris and Papadopoulos [16] investigated coupled vibration response between bending and longitudinal vibration by applying lateral excitation and measuring longitudinal vibrations on a rotating shaft with open crack assumptions. Using AFT and path following method, Sinou and Lees investigated the change of natural frequencies, harmonic components and evolution of orbital pattern of the cracked rotor at half the critical speed [17]. Pu et al. [18] established quasi-periodic vibrations of a cracked rotor on flexible bearings by harmonic balance method. Recently, model-based approach to identification of crack has also been attempted [19,20]. The approach is based on the premise that a fault induced change in the vibration behaviour of an undamaged system can be assumed to have caused by the so-called virtual forces and moments (that are functions of various fault parameters) acting on the undamaged system. The process of detection through an iterative procedure not only identifies but also locates the fault and its severity.

Parallel to the cracks in rotors, modelling of the cracks in beams with their breathing behaviour and associated nonlinearities have been investigated with potential application in structural health monitoring [21]. Pugno et al. [22] investigated beam with several breathing cracks and used harmonic balance method to

estimate its nonlinear dynamic behaviour that yields superharmonics in the spectrum of the response signal. Darpe et al. [23] proposed a new stiffness model for a Jeffcott rotor with two breathing cracks and analysed the effect of different orientation angle between the breathing cracks on steady-state unbalance response of such rotor.

With the advent of new signal analysis techniques such as wavelet transform, researchers also attempted to propose different diagnostic methodologies for the rotor crack. Adewusi and Al-Bedoor [24] applied Wavelet Transform to experimental signal of propagating transverse crack to track the growth of important harmonic components of the rotor speed. Zou and Chen [25] made a comparative study on time–frequency feature of transient response of cracked rotor by Wigner–Ville distribution and wavelet transform. Wan et al. [26] carried out vibration analysis of cracked rotor sliding bearing system with rotor–stator rubbing by harmonic wavelet transform. Zou et al. [27] analysed the torsional vibrations of a rotor with transverse crack using switching crack model and time–frequency features of torsional vibrations of the rotor are presented using wavelet transform. Prabhakar et al. [28] investigated the use of continuous wavelet transforms (CWT) for crack detection and monitoring in a cracked rotor system during its transient passage through critical speed. Zhou et al. [29] proposed a new signal analysis scheme to isolate the effect of gravity and free vibration for analysing mainly the transient vibration response of the cracked rotor and were able to show that crack features are better revealed with the proposed scheme than the conventional Fourier transform.

Bachschmid et al. [30] modelled the vibration behaviour of reactor coolant pump shaft with a transverse crack by accounting for the thermal stresses and external forces, which influence the breathing mechanism. The harmonic balance approach in the frequency domain is used to calculate the different harmonic components. Zhu et al. [31] analysed the dynamic behaviour of cracked rotor supported on active magnetic bearing and concluded that the adaptive control with active magnetic bearing can mask the crack symptoms.

Huang et al. [32] studied the effect of crack depth, rotational speed and damping on the stability. It is observed that the deeper crack can endure instability at lower speed. Slight damping considerably influences the instability zones. Using energy approach and speed-dependent bearing characteristics, Wu and Huang [33] presented crack-detection analysis and proposed a technique of intersections of equiamplitude contours from multiprobes to locate the crack and estimate its depth. They also studied various effects of rotation speed, crack location, crack depth, and sensing position on the response amplitude and suggested a feasible crack location and depth detection technique using two probes sensing the $2x$ component [34]. Meng and Gasch [35] investigated stability and stability degree for a cracked rotor on different types of journal bearings. It has been shown that the unstable zones are rather insensitive to the type of bearing used and depends on the speed and degree of asymmetry.

Although the high level of bending stresses are encountered in the rotors used in industry, torsional stresses are also encountered in many applications and even in case of rotors with no apparent torsional loading. Short-circuiting at the terminals, faulty synchronization, line switching and load rejection etc., are some of the causes that lead to abnormal torque in generator and turbine shafts. Torsional loads can lead to the development of cracks in rotors that are not transverse but oblique to the shaft axis. Such oblique crack is referred in the literature as slant crack.

Relatively less work is reported on slant crack in the rotor during the past 3 decades of research on cracked rotors. Ichimonji and Watanabe [36] investigated response of the rotor with slant crack. They modelled the rotor with a differential equation with parametric excitation assuming the slant crack opens and closes synchronously with torsional excitation frequency. However, only qualitative study was carried out. Later Ichimonji et al. [37] presented quantitative analysis using 3D FE model. Sekhar and Prasad [38] also presented FEM analysis by deriving first the flexibility matrix on similar lines as the work of Papadopoulos and Dimarogonas [15] and then making use of this matrix in the FE model of the rotor with slant crack. The breathing of the crack is modelled by assuming the stiffness variation of the rotor by a truncated cosine series. The stiffness matrix is assumed to vary synchronously with frequency of torsional excitation. The vibration response is then analysed under unbalance and torsional excitation. Prabhakar et al. [39] analysed transient lateral vibration response of the slant cracked rotor passing through its critical speed subjected to harmonic torsional excitation using FE model of the system. They showed presence of super and sub harmonic frequency components separated by an interval frequency that matches the torsional excitation frequency in the frequency response of the rotor, which they proposed can be used to detect slant crack. Sekhar et al. [40]

compared response of transverse and slant cracks. They proposed use of mechanical impedance for detection and monitoring of cracks although it was observed that slant crack are less sensitive to mechanical impedance. Breathing in case of slant crack is shown to depend on the torsional excitation frequency.

This paper deals with a Jeffcott rotor with slant crack. A flexibility matrix for such a rotor is derived based on fracture mechanics concepts and then used in the simple Jeffcott rotor model limiting only to lateral and axial degrees of freedom for analysing the response of such rotor to only unbalance excitation. Comparison with the Jeffcott rotor with transverse crack is carried out. The focus of the paper is on deriving a flexibility matrix for a slant crack based on fracture mechanics concepts and to bring out possible distinctive steady state unbalance response features for the transverse and slant cracks without resorting to any additional external torsional excitation as done in earlier studies [36–40]. In earlier studies on slant crack, the equations of motion are modelled with torsional excitation along with the unbalance excitation. It is also then assumed that the crack breathes synchronously with torsional excitation. In the present study, response-dependent nonlinear breathing crack model is considered and under the unbalance excitation, the gravity and dynamic forces acting on the rotor govern the breathing.

2. Flexibility of a rotor with slant crack

In this section, flexibility expression is derived based on strain energy density due to the presence of the crack and Castingliano's Theorem. Consider a shaft of radius R with a slant crack having a depth of a oriented at an angle of θ relative to the axis of the shaft (Fig. 1). Fig. 2 shows the details of the cross-section showing open and closed area of the crack above the crack edge. The shaft is loaded with axial force P_1, shear forces P_2 and P_3, bending moments P_4 and P_5 and torsional moment P_6. These forces act in a coordinate system 1–2–3 aligned along the shaft axis. The stresses due to these forces are resolved in another coordinate system aligned with the slant crack (1′–2′–3′) as shown in Fig. 1, which, compared to transverse crack, leads to more number of stress components responsible for the opening and tearing mode of crack displacement. For example, stress due to shear force P_2 in case of transverse crack does not contribute to the opening mode whereas in slant crack case, its component σ_2^{θ} in the coordinate system 1′–2′–3′ leads to opening mode of crack displacement

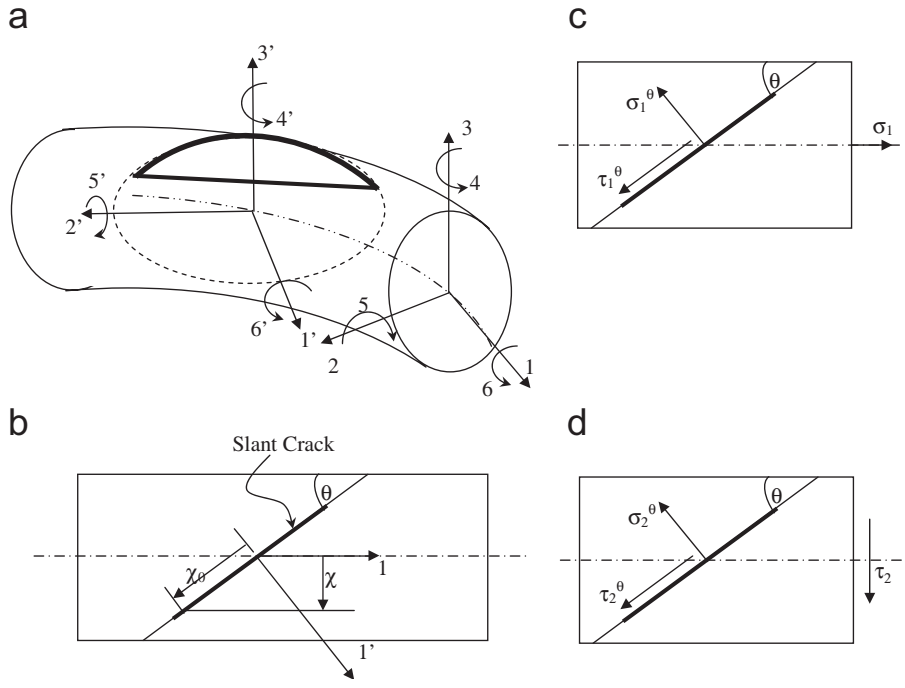

Fig. 1. Slant crack rotor with crack oriented at an angle θ with the axis and coordinate system.

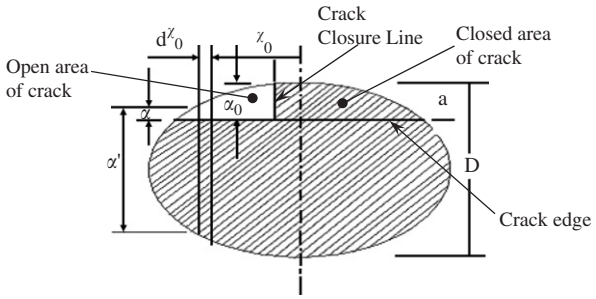

Fig. 2. Cross-sectional details of the slant crack rotor.

(Fig. 1d). Similarly, axial force P_1 leads to shear stress τ_1^{θ} causing tearing mode for slant crack, in addition to opening mode due to normal component of σ_1^{θ} (Fig. 1c).

The opening mode stress intensity factors are given as below:

$$K_1^{\mathrm{I}} = \sigma_1^{\theta}\sqrt{\pi\alpha}F_1 = \sigma_1 \sin^2\theta\sqrt{\pi\alpha}F_1 = \frac{P_1}{\pi R^2}\sin^2\theta\sqrt{\pi\alpha}F_1,$$

where α is depth of crack at any distance χ_0 from the centre along the crack edge (i.e., axis $2'$ in Fig. 1a) and α' is the total height of the strip of width $\mathrm{d}\chi_0$ (Fig. 2).

Similarly,

$$K_4^{\mathrm{I}} = \sigma_4^{\theta}\sqrt{\pi\alpha}F_1 = \sigma_4 \sin^2\theta\sqrt{\pi\alpha}F_1,$$

$$K_4^{\mathrm{I}} = \frac{4P_4\chi_0 \sin^3\theta}{\pi R^4}\sqrt{\pi\alpha}F_1,$$

$$K_5^{\mathrm{I}} = \sigma_5^{\theta}\sqrt{\pi\alpha}F_2 = \frac{4P_5}{\pi R^4}\sqrt{R^2-\chi_0^2\sin^2\theta}\sin^2\theta\sqrt{\pi\alpha}F_2. \tag{1}$$

The shear stress acting on the cross-section generate normal stress component along the slant crack direction causing opening mode crack displacement. Thus,

$$K_6^{\mathrm{I}} = \sigma_6^{\theta}\sqrt{\pi\alpha}F_2,$$

$$\sigma_6^{\theta} = \tau_6 \sin 2\theta,$$

$$\tau_6 = \frac{P_6\sqrt{R^2-\chi_0^2\sin^2\theta}}{(\pi/2R^4)},$$

$$K_6^{\mathrm{I}} = \frac{2P_6\sqrt{R^2-\chi_0^2\sin^2\theta}}{\pi R^4}\sin 2\theta\sqrt{\pi\alpha}F_2.$$

Similarly,

$$K_2^{\mathrm{I}} = \frac{kP_2}{\pi R^2}\sin 2\theta\sqrt{\pi\alpha}F_1,$$

$$K_3^{\mathrm{I}} = 0. \tag{2}$$

Sliding mode stress intensity factors are given below as

$$K_3^{\mathrm{II}} = \frac{kP_3}{\pi R^2}\sin\theta\sqrt{\pi\alpha}F_{\mathrm{II}},$$

$$K_6^{\mathrm{II}} = \frac{2P_6\chi_0 \sin^2\theta}{\pi R^4}\sqrt{\pi\alpha}F_{\mathrm{II}},$$

$$K_1^{\mathrm{II}}, K_2^{\mathrm{II}}, K_4^{\mathrm{II}}, K_5^{\mathrm{II}} = 0. \tag{3}$$

Tearing mode stress intensity factors are

$$K_1^{\mathrm{III}} = \tau_1^{\theta}\sqrt{\pi\alpha}F_{\mathrm{III}} \quad \text{where } \tau_1^{\theta} = \sigma_1 \sin\theta\cos\theta,$$

$$K_1^{\mathrm{III}} = \left(\frac{P_1}{\pi R^2}\sin\theta\cos\theta\right)\sqrt{\pi\alpha}F_{\mathrm{III}},$$

$$K_2^{\mathrm{III}} = \tau_2^{\theta}\sqrt{\pi\alpha}F_{\mathrm{III}} \quad \text{where } \tau_2^{\theta} = \tau_2\cos 2\theta,$$

$$K_2^{\mathrm{III}} = \frac{kP_2}{\pi R^2}\cos 2\theta\sqrt{\pi\alpha}F_{\mathrm{III}},$$

$$K_4^{\mathrm{III}} = \tau_4^{\theta}\sqrt{\pi\alpha}F_{\mathrm{III}}, \quad \tau_4^{\theta} = \sigma_4 \sin\theta\cos\theta,$$

$$K_4^{\mathrm{III}} = \frac{4P_4\chi_0 \sin^2\theta\cos\theta\sqrt{\pi\alpha}F_{\mathrm{III}}}{\pi R^4},$$

$$K_5^{\mathrm{III}} = \tau_5^{\theta}\sqrt{\pi\alpha}F_{\mathrm{III}}, \quad \tau_5^{\theta} = \sigma_5 \sin\theta\cos\theta,$$

$$K_5^{\mathrm{III}} = \frac{4P_5\sqrt{R^2 - \chi_0^2\sin^2\theta}}{\pi R^4}\sin\theta\cos\theta\sqrt{\pi\alpha}F_{\mathrm{III}},$$

$$\tau_6^{\theta} = \sigma_6\cos 2\theta,$$

$$K_6^{\mathrm{III}} = \frac{2P_6\sqrt{R^2 - \chi_0^2\sin^2\theta}}{\pi R^4}\cos 2\theta\sqrt{\pi\alpha}F_{\mathrm{III}}, \tag{4}$$

where

$$F_1(\alpha/\alpha') = \sqrt{\frac{2\alpha'}{\pi\alpha}\tan\left(\frac{\pi\alpha}{2\alpha'}\right)}\,\frac{0.752 + 2.02(\alpha/\alpha') + 0.37[1 - \sin(\pi\alpha/2\alpha')]^3}{\cos(\pi\alpha/2\alpha')},$$

$$F_2(\alpha/\alpha') = \sqrt{\frac{2\alpha'}{\pi\alpha}\tan\left(\frac{\pi\alpha}{2\alpha'}\right)}\,\frac{0.923 + 0.199[1 - \sin(\pi\alpha/2\alpha')]^4}{\cos(\pi\alpha/2\alpha')},$$

$$F_{\mathrm{II}}(\alpha/\alpha') = \frac{1.122 - 0.561(\alpha/\alpha') + 0.085(\alpha/\alpha')^2 + 0.18(\alpha/\alpha')^3}{\sqrt{(1 - (\alpha/\alpha'))}}$$

and

$$F_{\mathrm{III}}(\alpha/\alpha') = \sqrt{\frac{2\alpha'}{\pi\alpha}\tan\left(\frac{\pi\alpha}{2\alpha'}\right)}. \tag{5}$$

Using concepts of fracture mechanics, the additional strain energy due to crack is given by following expression:

$$U^c = \int_A J(A)\,\mathrm{d}A, \tag{6}$$

where $J(A)$ is strain energy density function and is expressed as

$$J(A) = \frac{1}{E'}\left[\left(\sum_{i=1}^{6} K_i^{\mathrm{I}}\right)^2 + \left(\sum_{i=1}^{6} K_i^{\mathrm{II}}\right)^2 + m_s\left(\sum_{i=1}^{6} K_i^{\mathrm{III}}\right)^2\right].$$

Here $E' = E/(1-\upsilon^2)$ and $m_s = 1+\upsilon$; υ is Poisson's ratio and K_i^{I} is the stress intensity factors corresponding to the opening mode of crack displacement, K_i^{II} the stress intensity factors corresponding to the opening mode of crack displacement and K_i^{III} the stress intensity factors corresponding to the opening mode of crack displacement.

Thus, the additional displacement of the shaft due to the presence of crack can be expressed as

$$u_i = \frac{\partial}{\partial P_i}\left[\iint J(A)\,\mathrm{d}A\right]. \tag{7}$$

Expressions of flexibility for the slant crack shaft can be given as

$$g_{ij} = \frac{\partial^2}{\partial P_i \partial P_j}\left[\frac{1}{E^1}\iint\left[\left(\sum_{1}^{6} K_i^{\mathrm{I}}\right)^2 + \left(\sum_{1}^{6} K_i^{\mathrm{II}}\right)^2 + m_s\left(\sum_{1}^{6} K_i^{\mathrm{III}}\right)^2\right]\mathrm{d}A\right] \tag{8}$$

and using the expressions for the SIF derived earlier, the coefficients of symmetric flexibility matrix can be expressed as

$$g_{11} = \frac{1}{E^1\pi R^4}\iint\left[2\alpha\sin^4\theta F_1^2 + 2m_s\alpha\sin^2\theta\cos^2\theta F_{\mathrm{III}}^2\right]\mathrm{d}A,$$

$$g_{22} = \frac{1}{E^1\pi R^4}\iint\left(2k^2\alpha\sin^2 2\theta F_1 + 2m_s k^2\alpha\cos^2 2\theta F_{\mathrm{III}}^2\right)\mathrm{d}A,$$

$$g_{33} = \frac{1}{E^1}\iint\frac{2k^2\sin^2\theta\alpha F_{\mathrm{II}}^2}{\pi R^4}\,\mathrm{d}A,$$

$$g_{44} = \frac{1}{E\pi R^8}\iint\left(\left(32\chi_0^2\sin^6\theta\alpha F_1^2 + 32m_s\chi_0^2\sin^4\theta\cos^2\theta\alpha F_{\mathrm{III}}^2\right)\right)\mathrm{d}A,$$

$$g_{55} = \frac{1}{E\pi R^8}\iint\left(32\left(R^2-\chi_0^2\sin^2\theta\right)\sin^4\theta\alpha F_2^2 + 32m_s\left(R^2-\chi_0^2\sin^2\theta\right)\sin^2\theta\cos^2\theta\alpha F_{\mathrm{III}}^2\right)\mathrm{d}A,$$

$$g_{66} = \frac{1}{E\pi R^8}\iint\left[8(R^2-\chi_0^2\sin^2\theta)\sin^2 2\theta\alpha F_2^2 + 8\chi_0^2\sin^4\theta\alpha F_{\mathrm{II}}^2 + 8m_s\left(R^2-\chi_0^2\sin^2\theta\right)\cos^2 2\theta\alpha F_{\mathrm{III}}^2\right]\mathrm{d}A,$$

$$g_{12} = \frac{1}{E^1}\iint\left[\frac{2k\sin^2\theta\,\sin\,2\theta\alpha F_1^2}{\pi R^4} + 2m_s k\frac{\sin\,\theta\,\cos\,\theta\,\cos\,2\theta\alpha F_{\mathrm{III}}^2}{\pi R^4}\right]\mathrm{d}A,$$

$$g_{13} = 0,$$

$$g_{14} = \frac{1}{E^1}\iint\left[\frac{8\chi_0\sin^5\theta\alpha F_1^2}{\pi R^6} + 8m_s\frac{\chi_0\sin^3\theta\cos^2\theta\alpha F_{\mathrm{III}}^2}{\pi R^6}\right]\mathrm{d}A,$$

$$g_{15} = \frac{1}{E^1}\iint\left[\frac{8\sin^4\theta\alpha F_1 F_2\sqrt{\left(R^2-\chi_0^2\sin^2\theta\right)}}{\pi R^6} + 8m_s\frac{\sqrt{\left(R^2-\chi_0^2\sin^2\theta\right)}\sin^2\theta\cos^2\theta\alpha F_{\mathrm{III}}^2}{\pi R^6}\right],$$

$$g_{16}=\frac{1}{E^1}\iint\left[\frac{4\sqrt{(R^2-\chi_0^2\sin^2\theta)}\sin^2\theta\ \sin\ 2\theta\alpha F_1F_2}{\pi R^6}+\frac{4m_s\sqrt{(R^2-\chi_0^2\sin^2\theta)}\ \sin\ \theta\ \cos\ \theta\ \cos\ 2\theta\alpha F_{\mathrm{III}}^2}{\pi R^6}\right]\mathrm{d}A,$$

$$g_{23}=0,$$

$$g_{24}=\frac{1}{E^1}\iint\left[\frac{8k\chi_0\ \sin\ 2\theta\alpha F_1^2\sin^3\theta}{\pi R^6}+8m_sk\frac{\chi_0\alpha\ \cos\ 2\theta\sin^2\theta\ \cos\ \theta F_{\mathrm{III}}^2}{\pi R^6}\right]\mathrm{d}A,$$

$$g_{25}=\frac{1}{E^1}\iint\left[\frac{8k\sqrt{(R^2-\chi_0^2\sin^2\theta)}\ \sin\ 2\theta\sin^2\theta\alpha F_1F_2}{\pi R^6}+8m_sk\frac{\sqrt{(R^2-\chi_0^2\sin^2\theta)}\ \sin\ \theta\ \cos\ \theta\ \cos\ 2\theta\alpha F_{\mathrm{III}}^2}{\pi R^6}\right]\mathrm{d}A,$$

$$g_{26}=\frac{1}{E^1}\iint\left(\frac{4k\alpha\sqrt{(R^2-\chi_0^2\sin^2\theta)}\sin^2 2\theta F_1F_2}{\pi R^6}+4m_sk\frac{\sqrt{(R^2-\chi_0^2\sin^2\theta)}\,\alpha\cos^2 2\theta F_{\mathrm{III}}^2}{\pi R^6}\right)\mathrm{d}A,$$

$$g_{36}=\frac{1}{E^1}\iint\frac{4k\chi_0\sin^3\theta\alpha F_{\mathrm{II}}^2}{\pi R^6}\,\mathrm{d}A,$$

$$g_{45}=\frac{1}{E^1}\iint\left[\frac{32\chi_0\sin^5\theta\alpha\sqrt{(R^2-\chi_0^2\sin^2\theta)}F_1F_2}{\pi R^8}+\frac{32m_s\chi_0\sqrt{(R^2-\chi_0^2\sin^2\theta)}\sin^3\theta\cos^2\theta\alpha F_{\mathrm{III}}^2}{\pi R^8}\right]\mathrm{d}A,$$

$$g_{46}=\frac{1}{E^1}\iint\left[\frac{16\chi_0\sin^3\theta\alpha\ \sin\ 2\theta F_1F_2\sqrt{(R^2-\chi_0^2\sin^2\theta)}}{\pi R^8}+\frac{16m_s\chi_0\sqrt{(R^2-\chi_0^2\sin^2\theta)}\sin^2\theta\ \cos\ \theta\ \cos\ 2\theta\alpha F_{\mathrm{III}}^2}{\pi R^8}\right]\mathrm{d}A,$$

$$g_{56}=\frac{1}{E^1}\iint\left[\frac{16\sin^2\theta\alpha\ \sin\ 2\theta F_2^2(R^2-\chi_0^2\sin^2\theta)}{\pi R^8}+\frac{16m_s(R^2-\chi_0^2\sin^2\theta)\ \sin\ \theta\ \cos\ 2\theta\ \cos\ \theta\alpha F_{\mathrm{III}}^2}{\pi R^8}\right]\mathrm{d}A. \tag{9}$$

If $\theta = 90^\circ$, the crack represents transverse crack and the above equations reduce to the flexibility expressions given in Appendix A. This Eq. (A.1) when converted to non-dimensional form are similar to those derived by Papadopoulos and Dimarogonas [15] for a transverse crack. For a general orientation of crack, the flexibility matrix of slant crack rotor is given by

$$[g]=\begin{bmatrix} g_{11} & g_{12} & 0 & g_{14} & g_{15} & g_{16}\\ g_{21} & g_{22} & 0 & g_{24} & g_{25} & g_{26}\\ 0 & 0 & g_{33} & 0 & 0 & g_{36}\\ g_{41} & g_{42} & 0 & g_{44} & g_{45} & g_{46}\\ g_{51} & g_{52} & 0 & g_{54} & g_{55} & g_{56}\\ g_{61} & g_{62} & g_{63} & g_{64} & g_{65} & g_{66} \end{bmatrix}, \tag{10}$$

which is found to be more populated compared to that of transverse crack [15]. It may be mentioned that the flexibility matrix of slant crack derived in Ref. [38] has same number of flexibility coefficients as the transverse crack (i.e., it is as populated as transverse crack) but with different expressions compared to those for a transverse crack given in Ref. [15]. In contrast the flexibility matrix derived here exhibits additional cross-coupled flexibility coefficients (g_{12}, g_{16}, g_{24}, g_{25}, g_{46} and g_{56}) that are absent for a transverse crack. The additional flexibility coefficients are expected because of the orientation of the surface crack relative to the shaft axis. For example, g_{12} flexibility coefficient represents coupling of axial and shear deflection is an additional cross-flexibility coefficient in case of slant crack. Observing Fig. 1c, any axial force along direction 1

is expected to generate shear deflection along 2 because of the oblique orientation of the slant crack. In case of transverse crack g_{12} is not expected because of the symmetry of shaft section containing the crack about an axis perpendicular to the crack edge.

For a 15 mm diameter shaft and crack depth ratio $\bar{a}$ (i.e., a/D) of 0.3, the above flexibility coefficients for a slant crack are evaluated for different slant crack angles. Fig. 3 shows the variation in flexibility when slant crack angle is varied from $\theta = 30^\circ$ to 90°. It may be noted that when oblique crack is oriented with $\theta = 90^\circ$, it represents a transverse crack.

Fig. 3 shows that the flexibility values g_{11}, g_{33}, g_{44}, g_{55} and g_{15} continuously increase as the orientation of crack changes from $\theta = 30^\circ$ (aligned more to the axis) to $\theta = 90^\circ$ (aligned across the axis), whereas, the flexibility values g_{12}, g_{16}, g_{22}, g_{26}, g_{25}, g_{66} and g_{56} continuously decrease. The axial flexibility (due to g_{11}) of a shaft with transverse crack is more compared to a shaft with slant crack of same depth. Similarly, the shaft with transverse crack is more flexible in bending (due to g_{44} and g_{55}) compared to the shaft with slant crack. However, the slant crack shows greater flexibility in torsion (due to g_{66}) compared to the transverse crack, particularly for $\theta < 60^\circ$. The above 12 flexibility coefficients have nonzero value for the fully open crack condition; the remaining 5 flexibility coefficients of the symmetric flexibility matrix (Eq. (11)) have a zero value for the fully open crack state.

For a shaft subjected to twisting moment excitation, the most probable orientation for a slant crack is $\theta = 45^\circ$, for which the flexibility expressions reduce to those given in Appendix A. A comparison of dimensionless flexibility values (corresponding to the fully open crack state) of slant crack (Eq. (A.3), given in Appendix A) with those of transverse crack is shown in Fig. 4. It may be observed that for g_{11}, g_{44}, g_{55}, g_{15} and g_{33}, the value of flexibility coefficients for the slant crack is less compared to those for the transverse crack. However, the value of flexibility coefficients for the slant crack is more compared to those for the transverse crack for g_{26}, g_{66} (involving torsion) and g_{22}. The flexibility coefficients g_{12}, g_{25}, g_{16} and g_{56} do not exist for the transverse crack (which is also observed in Fig. 3 for $\theta = 90^\circ$) and are shown in Fig. 4 only for the slant crack. It may be mentioned that the flexibility coefficients continuously change depending on the amount of open area of the crack that keeps changing due to the breathing phenomenon.

3. Unbalance vibration response of rotor with slant crack

Coupled axial and lateral vibration response of a Jeffcott rotor is investigated for both the slant and transverse crack cases. Consider a massless elastic shaft of length 0.7 m and diameter 15 mm with a disc of mass $m = 1$ kg at the centre of the span. The coordinates y, z and ξ, η represent the stationary and rotating axes, respectively, as shown in Fig. 5. It may be noted that the actual location of the slant crack is at an angle θ to the transverse plane (Fig. 1c). Hence, crack area in the rotor cross-section in Fig. 5 represents the projected view of the slant crack in transverse plane. $\varphi(t)$ is the angle of rotation and ω is the constant rotational speed. Angle β represents orientation of unbalance with respect to the crack direction (ξ direction), ε is the eccentricity of centre of mass at the disc location and c is damping coefficient. Considering direct stiffnesses k_ξ, k_η and k_u in the ξ, η and u directions, and cross-coupled stiffnesses $k_{\xi\eta}$, $k_{\eta\xi}$, $k_{\xi u}$, $k_{\eta u}$, $k_{u\xi}$, and $k_{u\eta}$, which come into play due to partial opening of the crack, the equations of motion can be expressed in the rotating coordinates as

$$\begin{aligned} &m(\ddot{\xi} - 2\omega\dot{\eta} - \omega^2\xi) + c\left(\dot{\xi} - \omega\eta\right) + k_\xi\xi + k_{\xi\eta}\eta + k_{\xi u}u = m\varepsilon\omega^2\cos\beta - mg\cos\varphi,\\ &m(\ddot{\eta} + 2\omega\dot{\xi} - \omega^2\eta) + c(\dot{\eta} + \omega\xi) + k_{\eta\xi}\xi + k_\eta\eta + k_{\eta u}u = m\varepsilon\omega^2\sin\beta + mg\sin\varphi,\\ &m\ddot{u} + c\dot{u} + k_{u\xi}\xi + k_{u\eta}\eta + k_u u = 0. \end{aligned} \tag{11}$$

Stiffnesses in the equations of motion are response dependent, resulting in nonlinear differential equations. The stiffness can be evaluated from the flexibility expressions given earlier.

Owing to the breathing of the crack, the stiffness continuously changes during the rotation of the rotor. The stiffness depends on the amount of open part of the crack. As shown in Fig. 2, an imaginary vertical line, referred as the crack closure line (CCL), can be assumed to separate the open (unshaded blank) area of the crack from the closed (shaded) area above the edge of the crack. As the rotor rotates, due to the forces acting on the rotor, the open area of the crack changes and so does the CCL position. This is illustrated in Fig. 6 for

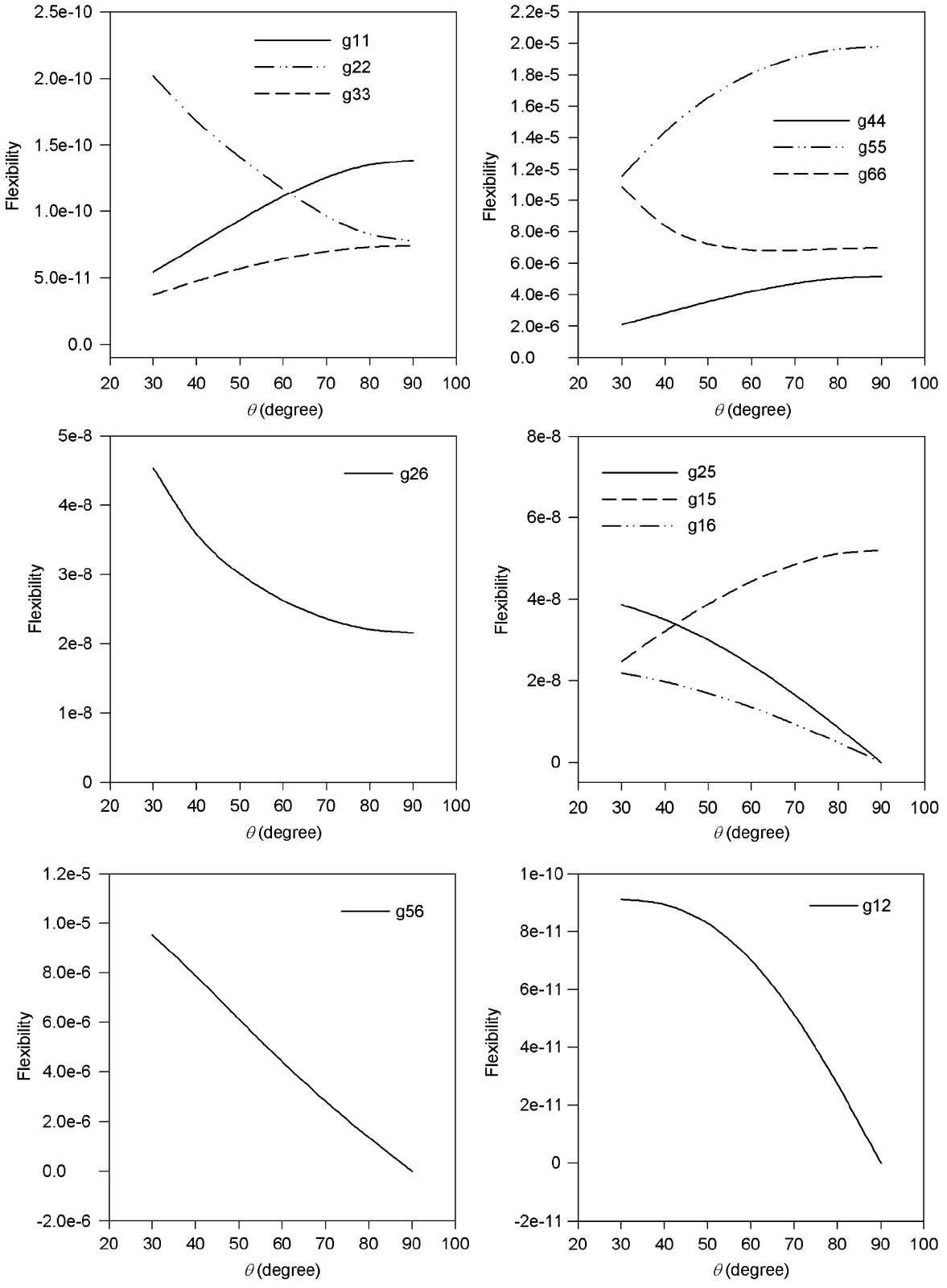

Fig. 3. Variation of flexibility coefficients with crack orientation angle.

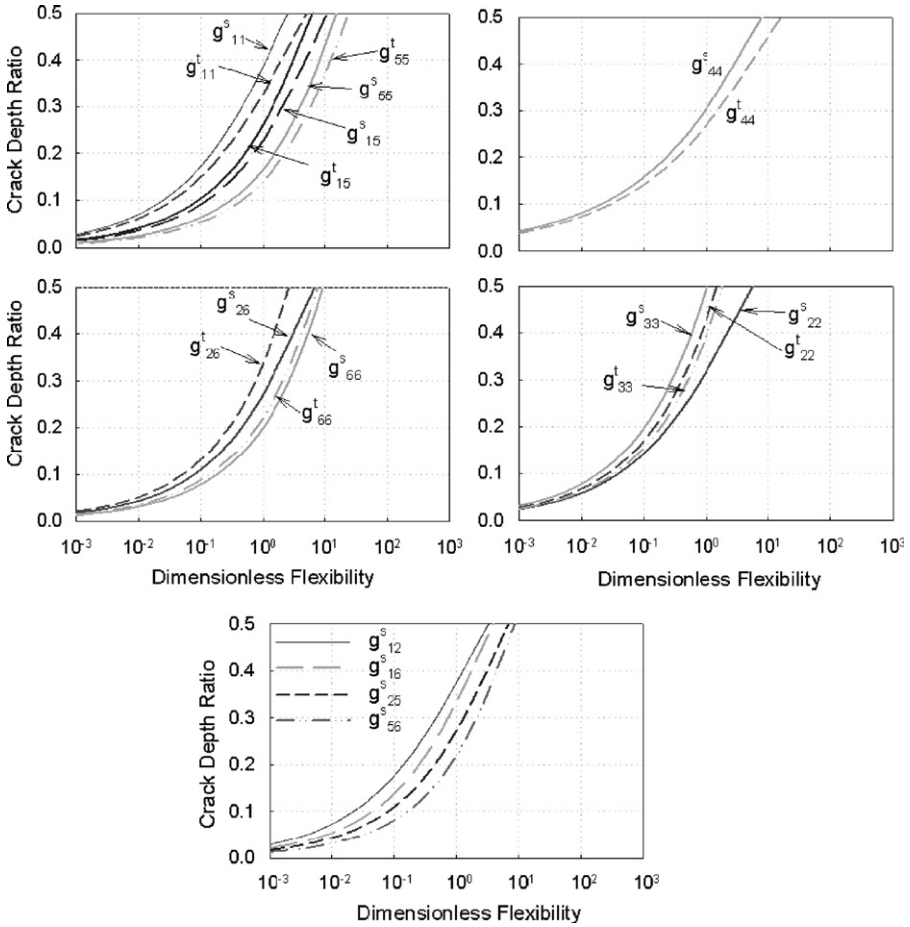

Fig. 4. Dimensionless flexibility coefficients for transverse and slant crack (superscripts: *s*-slant; *t*-transverse; g_{12}, g_{25}, g_{16} and g_{56} only for slant crack).

the transverse crack [14]. The similar concept applies to the slant crack where the CCL can take position anywhere along the crack edge in the elliptical cross-section. The crack edge is divided into 50 points in the present case. The position of CCL keeps changing along the crack edge (say from 1 to 50 while opening from B to A and from 50 to 100 while closing from B to A) as the rotor rotates clockwise. CCLP of 50 indicates a fully open crack, whereas, CCLP of 0 or 100 indicates a fully closed crack condition.

The typical breathing behaviour in the form of continuous change in the stiffness of the cracked rotor is due to the opening and closing of the crack under the effect of gravity acting on the horizontal rotor. Due to the presence of gravity, the upper portion of the cracked rotor at the start of the rotation is under compression and the crack is closed. As the rotor continues to rotate and the gravity direction being constant, the upper part now comes in the lower tensile region causing the crack to open. The process repeats and a periodic crack opening and closing phenomenon called crack breathing results. In case of vertical rotors, such as those of nuclear reactors, the radial preload may work similar to the gravity and cause crack breathing. Without the gravity in horizontal rotors and preload in vertical rotors, the periodic crack opening and closing is not possible. The crack breathing results in continuous and periodic variation in stiffness of the rotor. In absence of periodic variation of stiffness the generation of higher harmonics ($2x$ and $3x$) is not possible. In absence of constant radial load such as gravity in horizontal rotors or radial preload due to fluid forces or misalignment in case of vertical rotors, the response of the rotor will be predominantly $1x$ and its amplitude will be governed by the orientation of the residual unbalance with respect to the crack. If the crack and unbalance are out-of-phase, the unbalance will try to keep the crack always closed and the rotor will behave as an uncracked rotor.

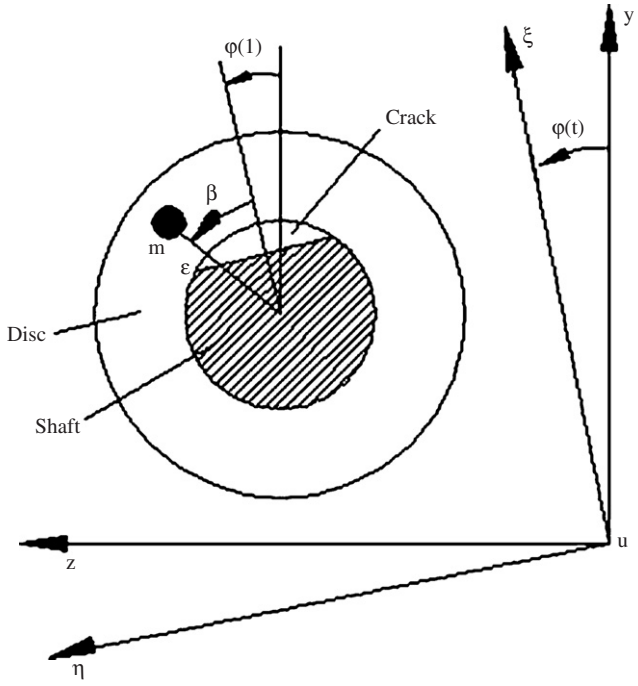

Fig. 5. Coordinate system.

Whereas, if the unbalance is in-phase with the crack, the unbalance may keep the crack always open and the amplitude level of $1x$ would be more compared to the uncracked rotor.

The variation of stiffness is shown in Fig. 7 comparing both the slant and transverse crack. The figure shows that the slant crack has a higher stiffness along ξ, u and η directions. Similarly the cross-stiffness coefficients $k_{\eta\xi}$, $k_{\xi u}$ and $k_{\eta u}$ are larger in value for transverse crack compared to the slant crack. Obviously the coupled lateral–longitudinal vibration response in case of slant crack is expected to be weak in comparison to the transverse crack.

Based on the stiffness values for the fully open crack state, the eigenvalue analysis of the cracked shaft is carried out for different crack depth ratios and the variation of the eigenvalues with crack depth is shown in Fig. 8. It may be observed that for the crack depth ratio of $\bar{a} = 0.1$ and less, there is no appreciable difference between slant and transverse crack as regards the drop in the eigenvalue of uncracked shaft. The drop is significant along ξ direction compared to the η direction for the lower crack depth range.

The coupled unbalance vibration response of cracked rotor for the two cases of slant and transverse crack is investigated. For evaluating the unbalance response, dimensionless eccentricity of $e = 0.1$ and damping ratio $(c/2m\omega_0)$ of 0.01 is considered. The vertical $(\bar{y})$, horizontal $(\bar{z})$ and axial $(\bar{u})$ response plotted in all the subsequent figures are non-dimensionalized quantities obtained by dividing the response by the static deflection of the rotor. Thus, $\bar{y} = y/\delta$, $\bar{z} = z/\delta$ and $\bar{u} = u/\delta$, where δ is the static deflection of the rotor. The orbit response at speed $r = 0.5$ is shown in Fig. 9 (dimensionless speed $r = \omega/\omega_0$, where ω_0 is the first bending critical speed). It may be noted that for the transverse crack the 3D orbit plot shows larger amplitude along the axial direction $(\bar{u})$ compared to the slant crack. Fig. 10 shows the time domain response for this case. The response in the lateral direction at this speed does not show an appreciable difference between the two cases of transverse and slant crack. For the axial direction, the slant crack rotor shows a marked reduction in the amplitude, although in both the cases, a high-frequency component of very small amplitude is observed in the axial response, which corresponds to the axial natural frequency (1150 Hz) of the rotor.

The radial unbalance excites the longitudinal vibration due to the cross-coupled stiffness in the equation of motion. The lower values of cross-coupled stiffnesses $k_{\xi u}$ and $k_{\eta u}$ for the case of slant crack (Fig. 7) generate a lower amplitude response in the axial direction, which is evident in Figs. 9 and 10.

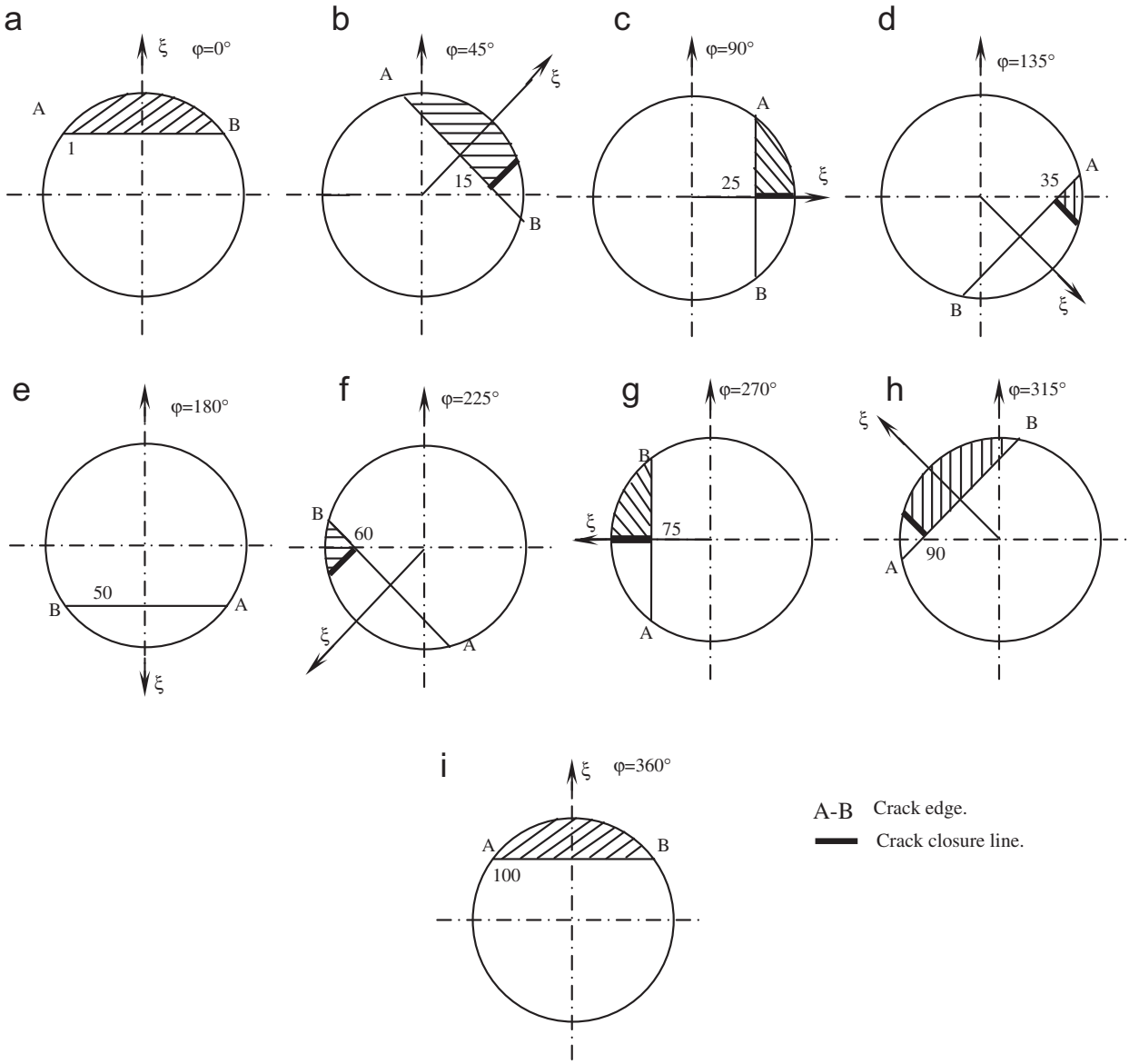

Fig. 6. Variation of crack closure line position with angular position of rotor [14].

The response of the cracked rotor at 1/3rd critical speed is important as the nonlinearity due to the crack breathing influence the response at this speed. The response of the crack at this speed is now analysed in frequency domain to ascertain the frequency content and its variation with crack depth for both the slant and transverse cracks. At this speed, the response of the rotor is governed more by the gravity than the unbalance excitation.

The unbalance response of the cracked rotor with slant crack and with transverse crack is found for different crack depth ratios and the frequency response is evaluated for each case. Fig. 11 shows the variation in the amplitudes of frequency components in the response of both slant and transverse crack rotor with crack depth. The figure shows that the 1x response for both slant and transverse cracks increases rapidly after the crack depth increases beyond 0.2 and the increase is more rapid for the vertical response than the horizontal. For both the vertical and horizontal response, the slant crack rotor shows lower value of response amplitude compared to the transverse crack. The difference between the two cases, however, increases with crack depth

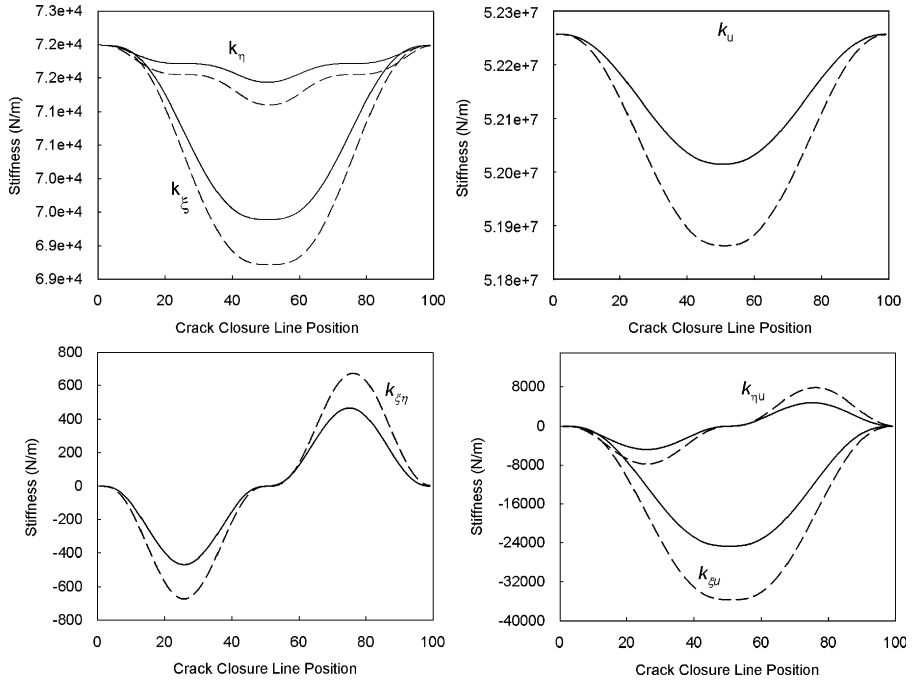

Fig. 7. Variation of stiffness in rotor fixed coordinates (ξ–η–u) with CCLP for slant crack (___) and transverse crack (- - -) for $\bar{a} = 0.3$.

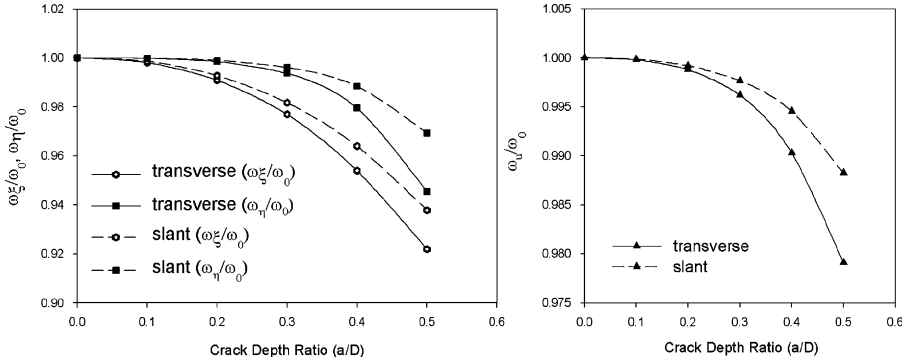

Fig. 8. Comparison of eigenvalues for transverse and slant crack rotor for different crack depth ratio.

ratio. It is prominently noticed that the $1x$ amplitude is stronger in vertical direction than in horizontal direction. The $2x$ amplitude variation shows that there is not much difference between the slant and transverse crack rotor response in this case. However, an important difference in this case (compared to $1x$ response) is that the horizontal response is greater (although marginally) than the response in vertical direction for both the types of crack. The increase in the amplitude of the $2x$ frequency component in both cases is more or less linear with crack depth compared to the previous case of $1x$ frequency components.

The variation of amplitudes of $3x$ frequency component is quite different. In this case, the amplitude of frequency components increase linearly up to the depth of 0.25 for vertical direction for both transverse and slant crack rotor. The amplitude of $3x$ frequency component in vertical direction drops beyond $\bar{a} = 0.3$ for the transverse crack as observed from Fig. 11 and the $3x$ amplitude at $\bar{a} = 0.4$ is even less than that for $\bar{a} = 0.15$. In addition, the gap between the amplitudes of vertical and horizontal direction closes at $\bar{a} = 0.4$ for transverse crack. The rate at which amplitudes increase in case of slant crack drops beyond $\bar{a} = 0.3$; however, the difference in amplitude between horizontal and vertical direction is fairly maintained beyond $\bar{a} = 0.3$.

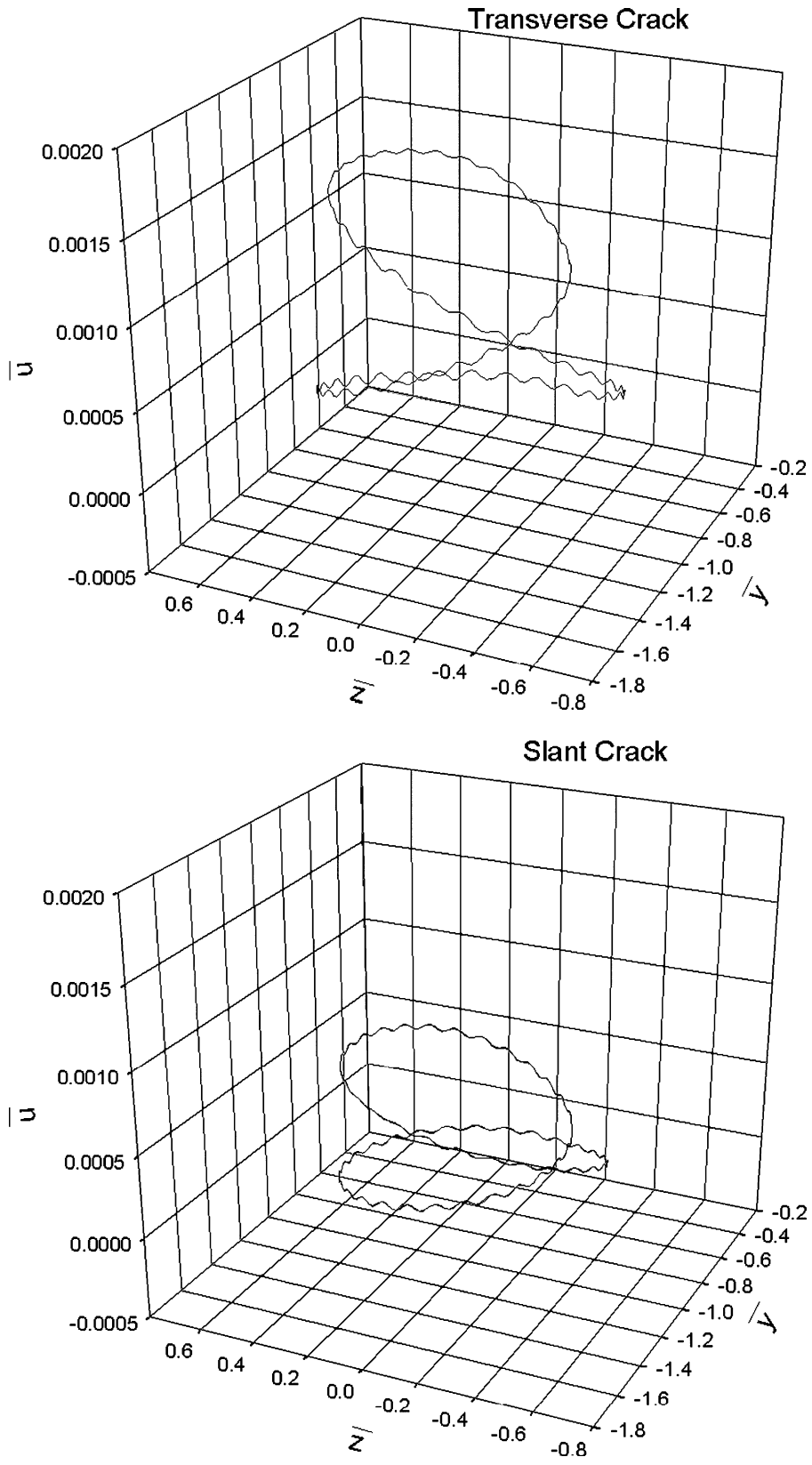

Fig. 9. Coupled axial–lateral dimensionless vibration response at $r = 0.5$.

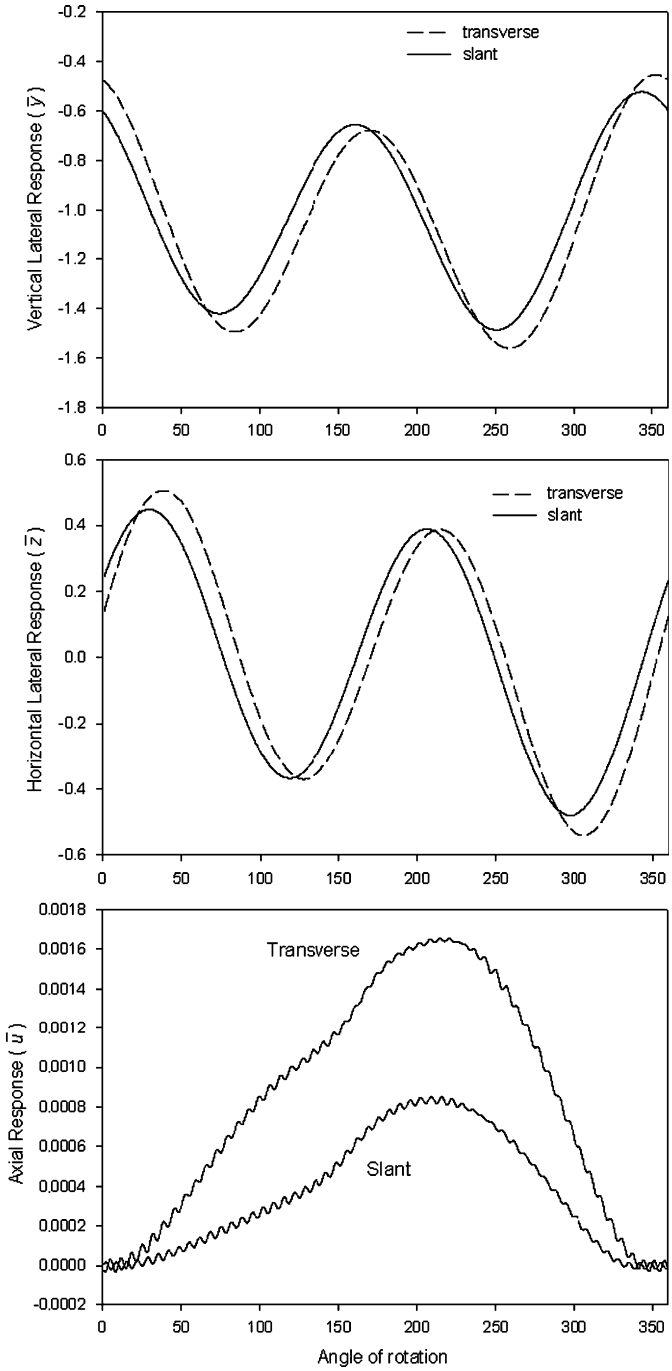

Fig. 10. Time domain coupled dimensionless vibration response at $r = 0.5$.

Amplitudes of higher harmonic components for crack depth up to $\bar{a} = 0.3$ in Fig. 11 show that although both $2x$ and $3x$ frequency components exhibit linear increase in the amplitudes with crack depth, the amplitude of $3x$ frequency component is much larger compared to that of $2x$ (e.g., 11 times larger (0.055 against 0.005) for transverse crack in horizontal direction). The stronger $3x$ amplitude can be very useful in trend monitoring of both types of cracks (transverse and slant) when it is shallow. During coast up operation of the rotor through 1/3rd critical speed, the frequency spectrum at this speed can be used to update the trend

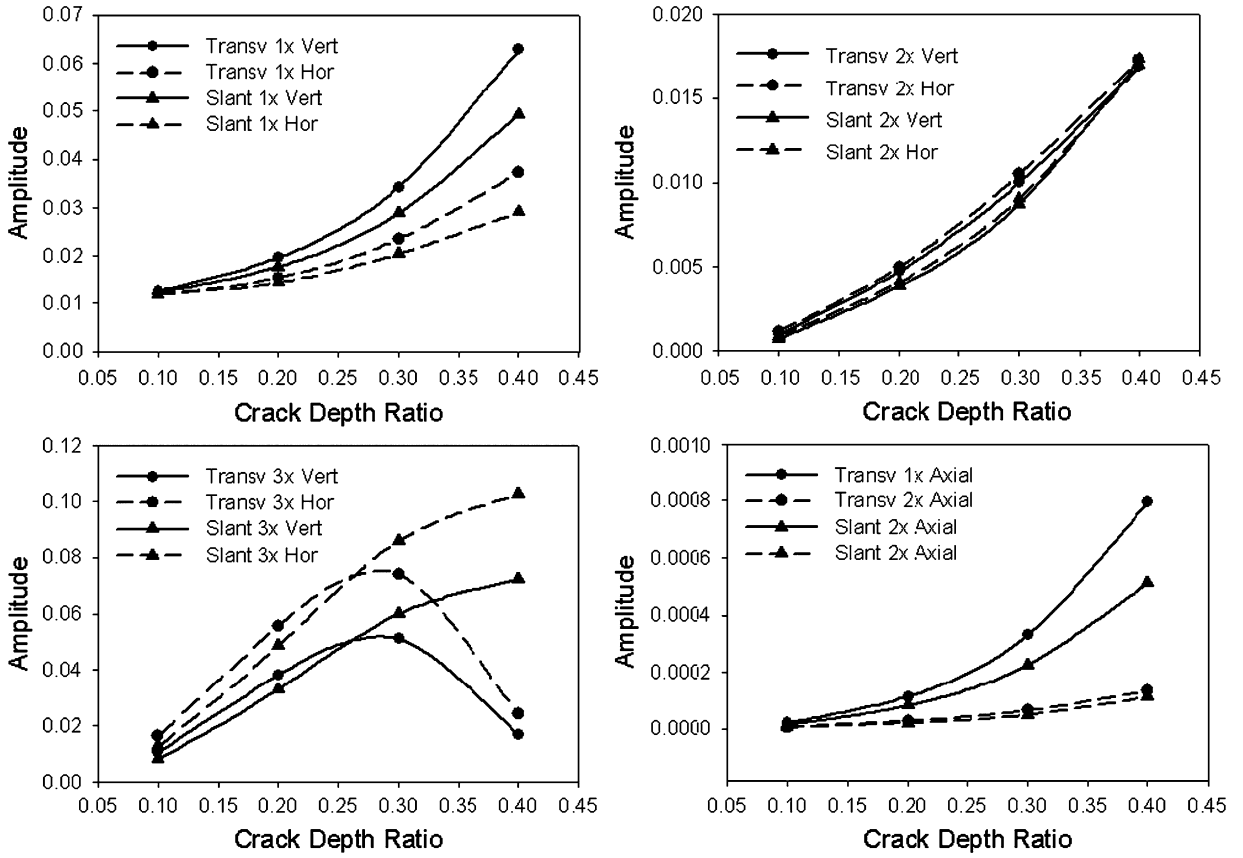

Fig. 11. Comparison of dimensionless amplitudes of frequency components in vertical ($\bar{y}$), horizontal ($\bar{z}$) and axial ($\bar{u}$) directions for the slant and transverse crack showing trend with crack depth ratio (for $r = 1/3$).

record of the amplitude of $3x$ frequency component. However, when the $3x$ component is not trended, it is difficult to diagnose the depth of the crack based on $3x$ amplitude from a solitary vibration signal reading because of the peculiar trend of the $3x$ amplitude after $\bar{a} = 0.3$ as seen in Fig. 11 (two different crack depths can yield the same amplitude $3x$ frequency component). In fact the amplitude of $3x$ component for transverse crack is almost the same for $\bar{a} = 0.1$ and 0.4. From the type of variation beyond $\bar{a} = 0.35$, wherein the amplitude of $3x$ component for transverse crack shows reduction by a significant amount compared to the continued increase of $3x$ amplitude for slant crack, it would be possible to distinguish the type of crack, slant or transverse.

The response in the axial direction shows that the $1x$ response increases with crack depth for both slant and transverse cracks. The $2x$ amplitude in axial direction does not show noticeable change even for larger depths for both types of cracks.

In the literature, the $3x$ amplitude variation with crack depth of the type observed in Fig. 11 is not reported. To understand the reason for the typical $3x$ amplitude variation observed, the stiffness variation of both slant and transverse crack rotor at the 1/3rd critical speed is analysed. Fig. 12 shows the stiffness variation in the vertical and horizontal directions of the transverse and slant crack for different crack depths. The figure also shows the frequency content of the stiffness variation in the vertical and horizontal directions. At lower depth of crack ($\bar{a} = 0.2$) the stiffness variation of the rotor in vertical direction shows very prominent $1x$ frequency component and comparatively smaller $2x$ and $3x$ frequency components. The stiffness variation in horizontal direction is such that the $1x$, $2x$ and $3x$ frequency components have approximately same amplitudes, with $3x$ frequency component far exceeding the amplitude of the corresponding vertical component. It may be noted

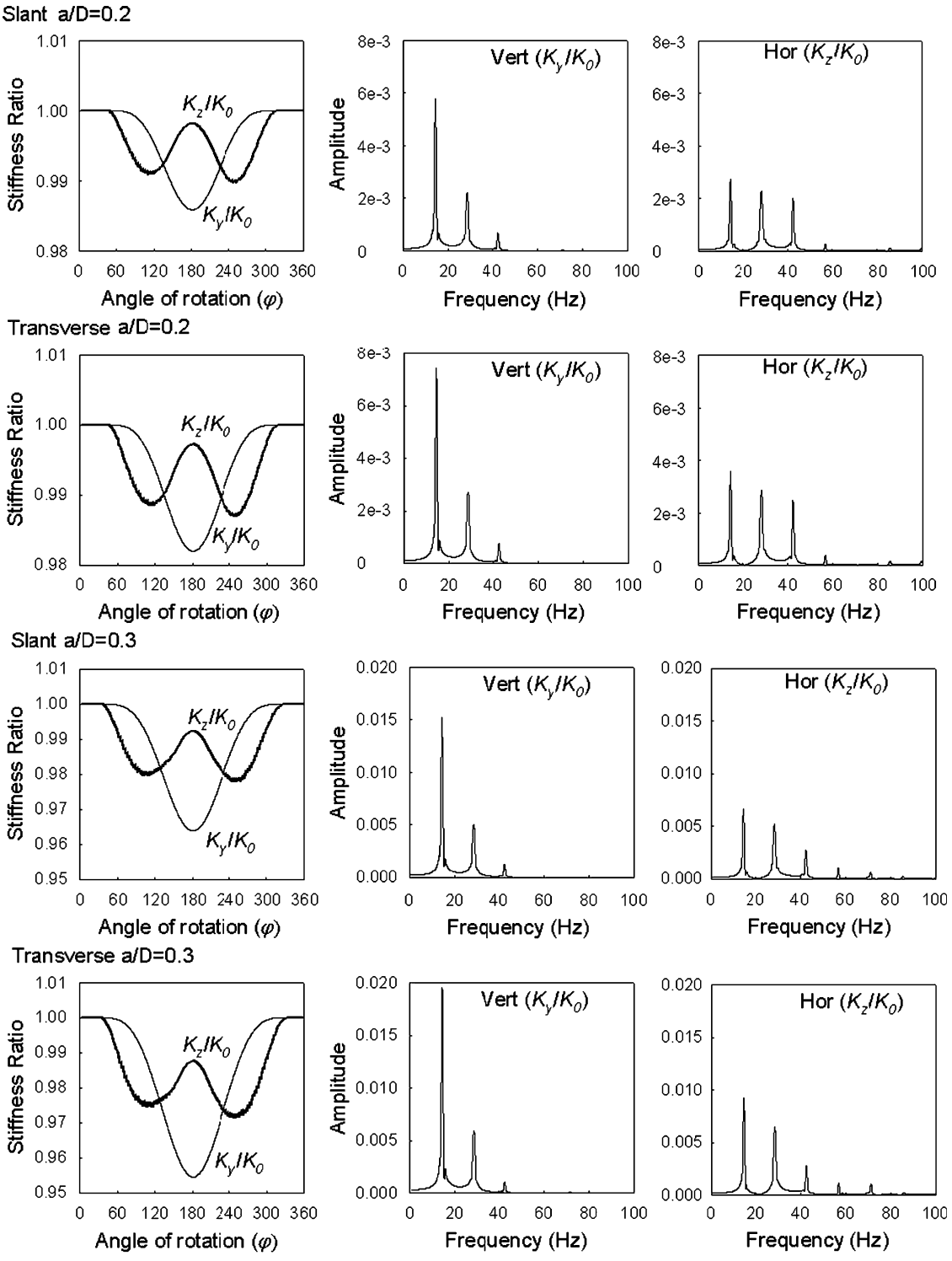

Fig. 12. Stiffness ratio (k_y/k_0, k_z/k_0) variation and its dimensionless frequency components.

that the existence of $3x$ excitation frequency (due to stiffness variation) matches with the bending critical speed and hence the bending natural frequency (42.7 Hz) is prominently observed in the spectra. The stronger $3x$ excitation frequency in horizontal direction leads to the presence of stronger bending natural frequency

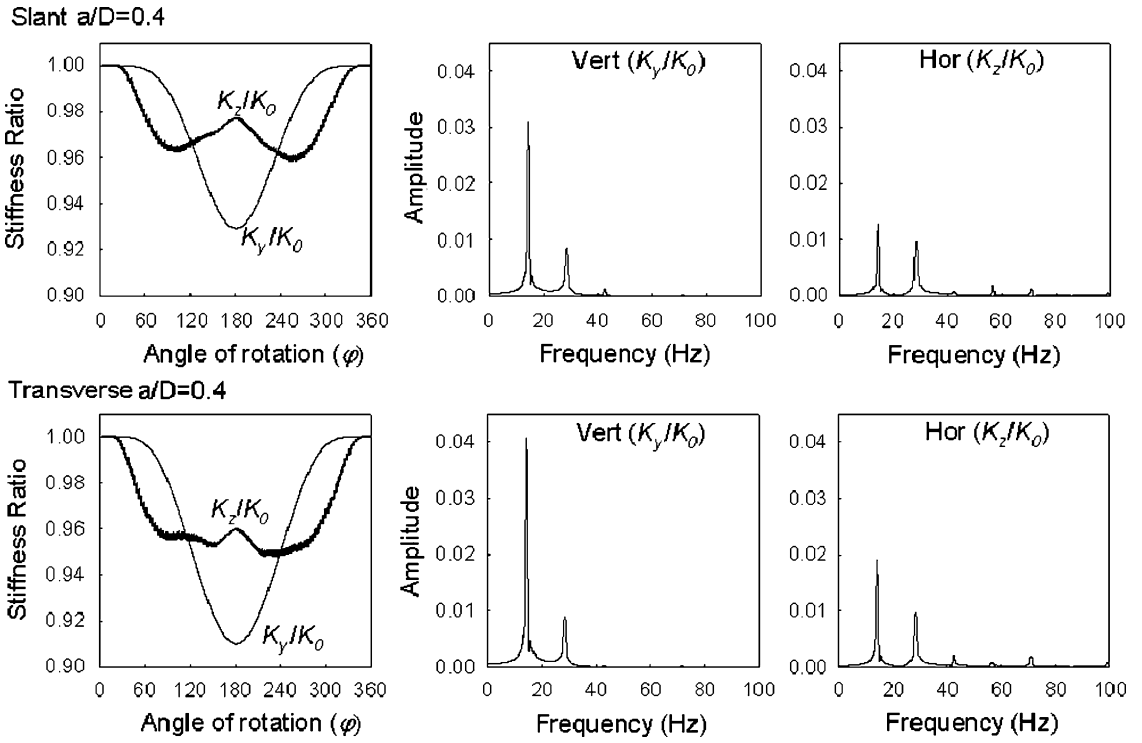

Fig. 12. (*Continued*)

component in horizontal direction in the response of the cracked rotor. Almost similar stiffness variation is observed for the transverse crack except for stronger $1x$ amplitude in vertical direction compared to the slant crack stiffness variation. This is reflected in the stronger $1x$ response amplitude for transverse crack compared to slant crack in Fig. 11.

At crack depth of $\bar{a} = 0.3$, the amplitudes of frequency components increase and more higher harmonic components (e.g. $5x$) show up in the horizontal direction in stiffness variation of both types of crack. The $3x$ amplitude in horizontal direction is still stronger in both types of crack. However, for crack depth of $\bar{a} = 0.4$, Fig. 12 shows significant changes in the stiffness variation in the vertical and horizontal direction of the cracked rotor. These changes influence the amplitudes of $3x$ harmonic components. Thus, the stiffness variation due to crack breathing could influence harmonic content of the response of the cracked rotor and a changed stiffness variation could be responsible for the type of $3x$ amplitude variation that is observed in Fig. 11.

In practice, an important parameter to consider is the orientation of unbalance with respect to the crack direction (ξ direction) shown as angle β in Fig. 5. The unbalance orientation angle is not known a priori and it is important to investigate the effect of this angle β on the amplitudes of the frequency components at 1/3rd critical speed investigated earlier in the section. The simulations at this speed is repeated at three different values of $\beta = 90^\circ$, 180° and 270°. The results are shown in Fig. 13 where it is clear that the amplitudes of $2x$ and $3x$ harmonic components do not change with unbalance orientation angle for both slant as well as transverse crack. Variation of amplitudes of $2x$ and $3x$ frequency components observed in Fig. 13 also shows that irrespective of the value of β, the variation of both these frequency components follow exactly the similar pattern as shown for $\beta = 0^\circ$ in Fig. 11. The results shown in Fig. 13 also corroborates with the fact that the higher harmonic components ($2x$, $3x$, etc.) are result of stiffness variation due to breathing of the crack and are not dependent on the phase of the unbalance relative to crack.

The $1x$ frequency component is predominantly due to the unbalance and additional flexibility of the rotor due to presence of crack, and hence there is a significantly stronger effect of β on the variation of amplitude of

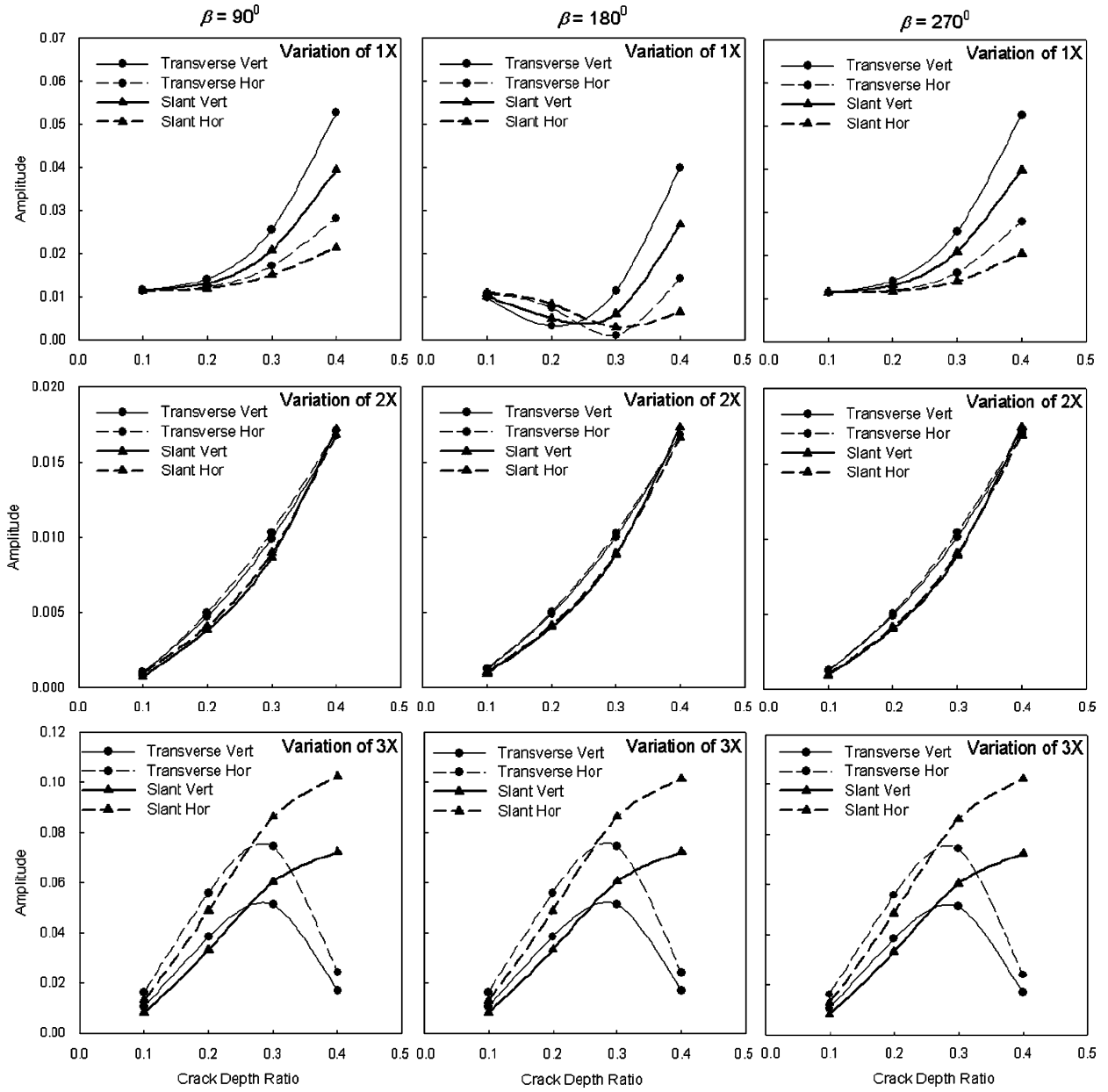

Fig. 13. Comparison of dimensionless amplitudes of frequency components for the slant and transverse crack for different values of β showing variation with crack depth ratio (for $r = 1/3$).

$1x$ frequency component, evident from Fig. 13. This effect is better indicated in Fig. 14 that shows for different crack depth ratios the effect of unbalance orientation angle. The figure shows that when the unbalance is oriented out-of-phase with the crack ($\beta = 180^\circ$), the amplitudes of $1x$ frequency component for both slant and transverse cracks in both horizontal and vertical directions drop compared to when unbalance is in-phase with the crack ($\beta = 0^\circ$).

The above results shows that only $1x$ frequency components are affected by orientation of unbalance relative to the crack direction and the higher harmonic components remain unaffected. It also means that irrespective of orientation of unbalance, the pattern of variation of amplitudes of $3x$ frequency component at 1/3rd critical speed can be utilized for detection of presence and type of crack (slant/transverse).

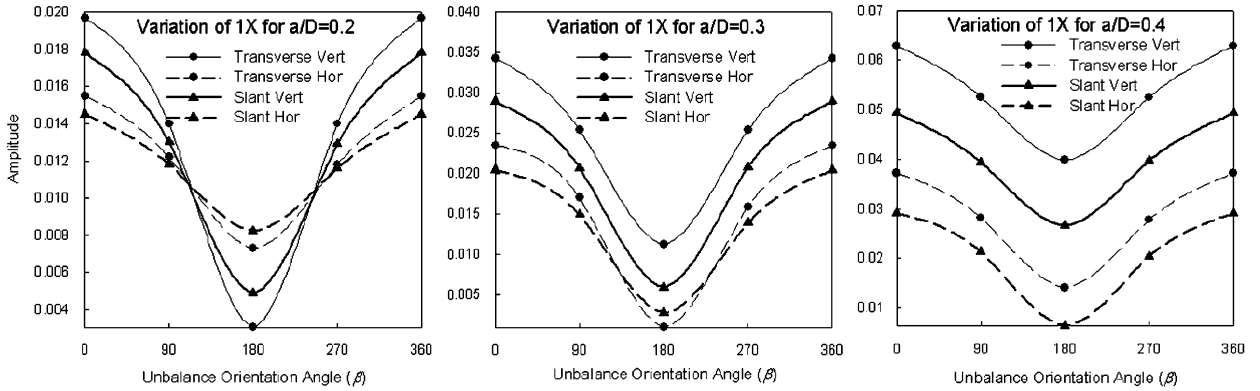

Fig. 14. Variation of dimensionless amplitude of $1x$ frequency components with unbalance orientation angle for different crack depths.

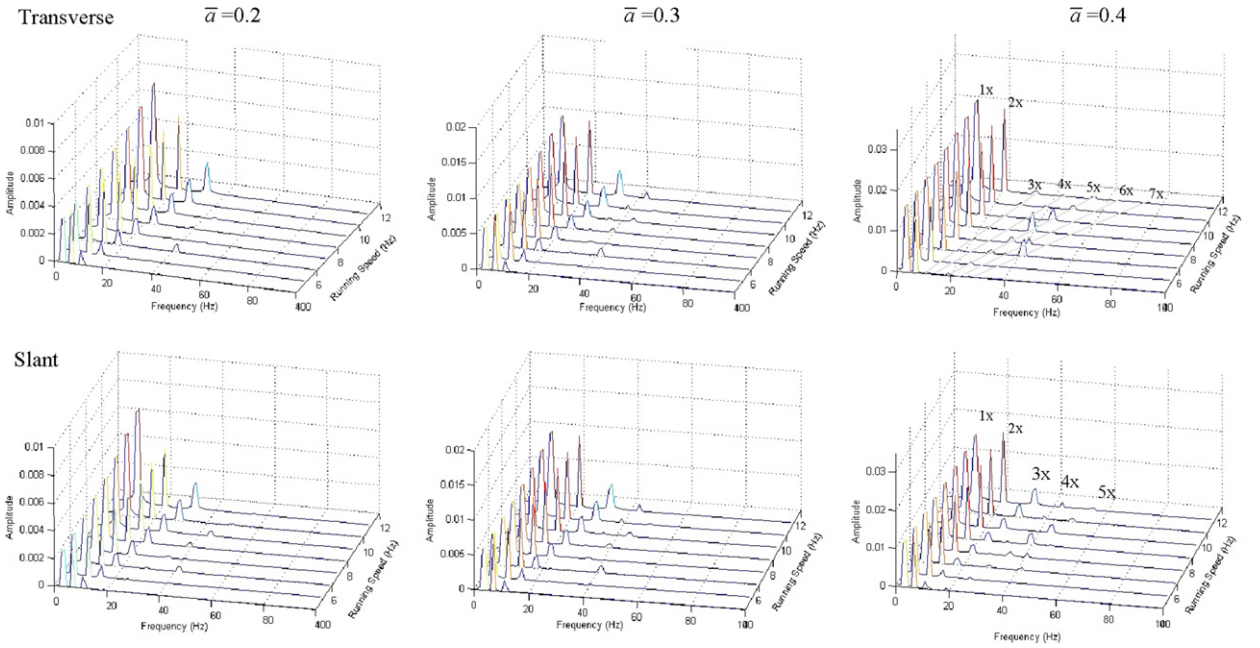

Fig. 15. Spectrum cascade plot of the dimensionless horizontal lateral vibration ($\bar{z}$) of the cracked rotor for different crack depths for speed range of 4–11 Hz showing subharmonic resonances at 1/5th, 1/7th the critical speed.

The spectrum cascade plot has been extensively used for fault identification. The evolution of amplitudes in vertical, horizontal and axial direction is now studied for both slant and transverse crack. Steady-state unbalance response at rotational speed ranging from 4 to 50 Hz in steps of 1 Hz is evaluated and plotted in the form of spectrum cascade plot. For the sake of clarity, the plot is divided into 3 regions; subcritical regions of 4–11 and 12–27 Hz and frequency range of 28–50 Hz that covers uncracked bending critical speed of 42.7 Hz. Fig. 15 shows horizontal vibration response of the cracked rotor at different crack depths in the first subcritical region. For $\bar{a} = 0.4$, the figure shows distinctive presence of subharmonic resonance at 1/5th critical speed (8.4 Hz) for both transverse and slant crack. The subharmonic resonance at 1/7th critical speed (6 Hz) is observed for transverse crack but not so prominently for the slant crack. A small amplitude peak is also observed at 7 Hz (1/6th critical speed) for both types of crack. At lower depths the resonances at 1/5th and 1/7th critical speed are less pronounced for both types of cracks. Another important observation from the spectrum cascade plots is lower amplitudes of $3x$ frequency component for transverse crack of depth ratio

$\bar{a} = 0.4$ compared to slant crack of same depth. Similar trends have been observed for the vertical vibration response (not shown here) with comparatively quite smaller amplitudes of higher harmonic components ($3x$, $5x$ and $7x$) for both types of crack to those shown in Fig. 15 for horizontal vibration. For both vertical and horizontal vibrations at 1/5th and 1/7th critical speeds, transverse crack exhibits stronger subharmonic resonance amplitudes compared to slant crack.

At the next frequency range of 12–27 Hz that covers two major subharmonic resonances at 1/3rd and $\frac{1}{2}$ critical speeds, the evolution of amplitudes of vibration of transverse and slant crack for different depths of crack is shown in Fig. 16. The figure shows that for transverse crack, the amplitude at 1/3rd subharmonic resonance (14 Hz) increases from $\bar{a} = 0.2$ to $\bar{a} = 0.3$ but drops for $\bar{a} = 0.4$. At all crack depths, transverse crack shows stronger subharmonic resonances compared to slant crack at $\frac{1}{2}$ critical speeds (21 Hz). In the third frequency region, the resonance at critical speed of 42.7 Hz is shown in Fig. 17. For the crack depths of $\bar{a} = 0.3$ and 0.4, unstable response has been obtained near 42 Hz and hence unbalance response at speeds close to 42 Hz is skipped in the spectrum cascade plots for both slant and transverse cracks. It is therefore not appropriate to compare the peak amplitudes at resonance for different crack depths between slant and transverse cracks. However, near the first bending critical speed, for all crack depths and types of crack, the response is predominantly $1x$ as observed from Fig. 17.

Fig. 18 shows the axial vibration response for speed range 4–50 Hz. The spectrum cascade plot shows continuous increase in the amplitude of $1x$ component before approaching the critical speed region (near 42 Hz) with a marginal increase in the amplitude near the subharmonic resonance at 21 Hz ($\frac{1}{2}$ the critical speed). In contrast, the amplitude of $2x$ frequency component remains almost constant with a slight rise at the $\frac{1}{2}$ subharmonic resonance. For both these frequency components, the amplitude is substantially reduced after the critical speed for a short speed range before the amplitudes pick up again. The trend is similar for all the crack depths and for both types of crack. However, for slant crack the amplitudes of the frequency components in the axial vibration are smaller compared to the transverse crack indicating stronger coupling between lateral and longitudinal vibrations for the later and the observation corroborates the results presented in Figs. 9 and 10.

The sudden drop in the axial response at the critical speed is related to the drop in the cross-coupled stiffness values. It is observed that at 43 Hz, just after the critical speed, the cross-coupled stiffness $k_{\xi u}$ and $k_{\eta u}$ drops to

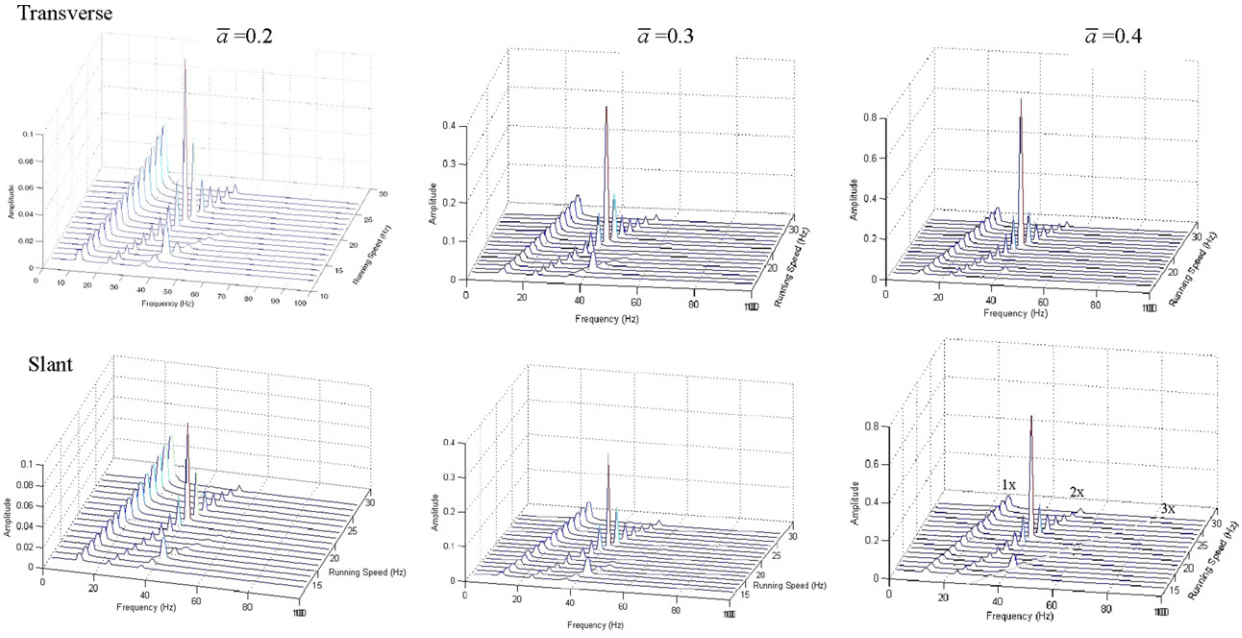

Fig. 16. Spectrum cascade plot of the dimensionless horizontal lateral vibration ($\bar{z}$) of the cracked rotor for different crack depths for speed range of 12–27 Hz showing subharmonic resonances at 1/3rd and 1/2 the critical speed.

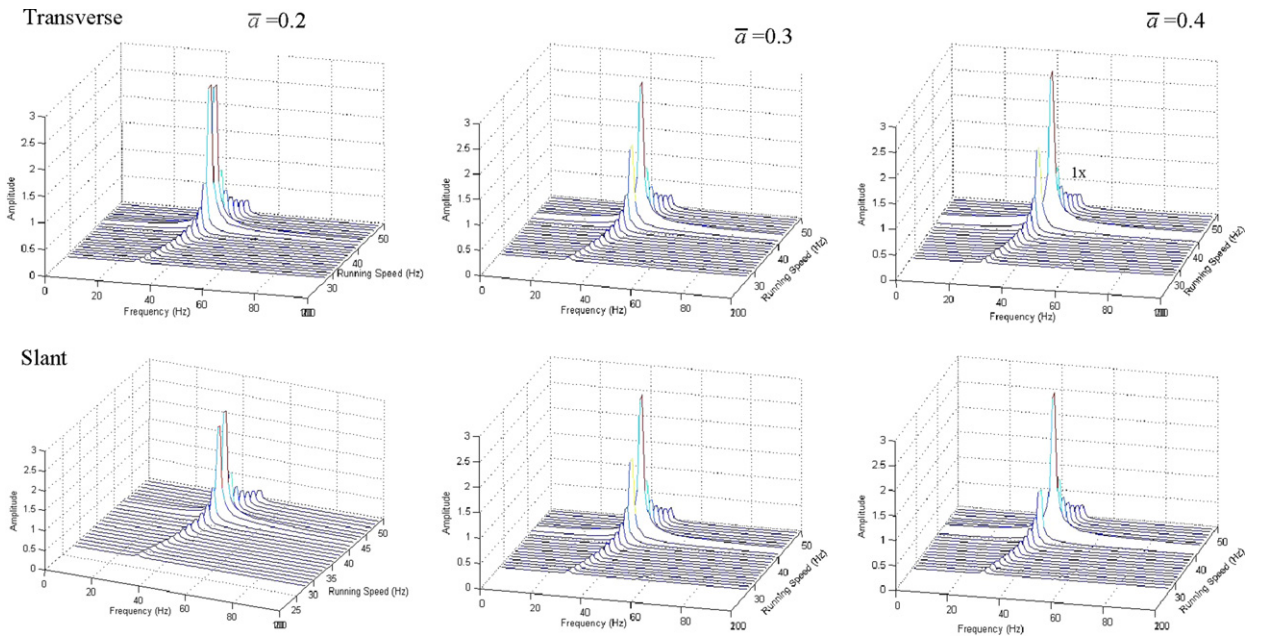

Fig. 17. Spectrum cascade plot of the dimensionless horizontal lateral vibration ($\bar{z}$) of the cracked rotor for different crack depths for speed range of 28–50 Hz showing resonance near first bending critical speed.

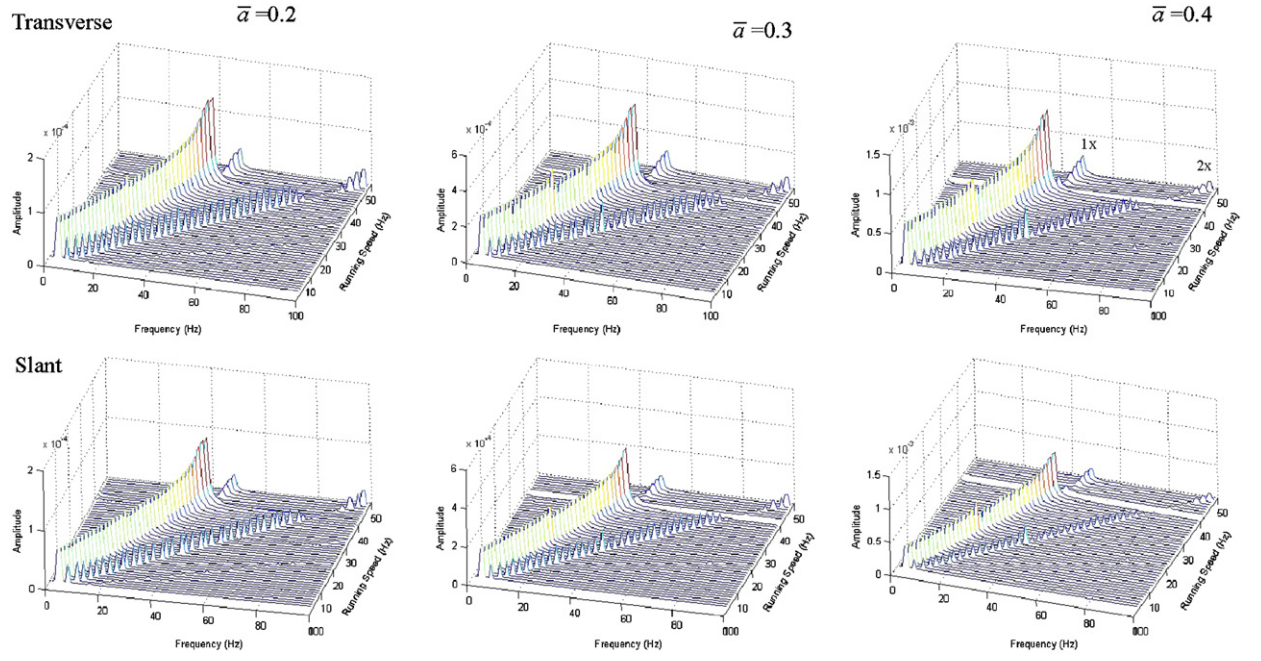

Fig. 18. Spectrum cascade plot of the dimensionless axial vibration ($\bar{u}$) of the cracked rotor for different crack depths.

less than 1/3rd of the corresponding values at subcritical region. In fact the direct stiffness k_{ξ} itself becomes almost equal to uncracked rotor stiffness, as the crack tends to close near this speed. The resulting reduced cross-coupled stiffness causes substantial drop in the cross-coupled response in the axial direction. This behaviour of the cracked rotor could be understood because of the nonlinear, response-dependent breathing

crack model and coupled vibration used in the study. The model helped in studying the direct and cross-coupled stiffness variation at all speeds and the speed-dependent and depth-dependent stiffness variation helped in understanding the nature of response observed in Figs. 11 and 18. It could also explain why higher harmonic components in horizontal direction in cracked rotors is stronger compared to the ones in vertical direction (Fig. 12). Most other crack models that are generally response independent and enforce periodic stiffness variation at all speeds would fail to show this behaviour of the cracked rotor.

4. Conclusions

The flexibility matrix of a slant crack has been derived. The flexibility matrix of the slant crack rotor is more populated and contains more non-zero off-diagonal elements than that of the rotor with transverse crack indicative of richer coupling mechanisms. Detail investigation of the variation of flexibility of the slant crack rotor with the angle of the crack with shaft axis is carried out. Flexibility coefficients are also compared with the case of rotor with transverse crack. The lateral and longitudinal stiffness of the rotor is more for the slant crack than for transverse crack.

The sensitivity analysis of using higher harmonics in the response of the rotor at 1/3rd critical speed for the detection of crack and its depth monitoring has been carried out. The amplitude of the $2x$ frequency component increases almost linearly and is suited for both detection and monitoring of crack. The amplitude of $3x$ frequency component shows a significantly different variation compared to the $1x$ and $2x$ components. Beyond crack depth ratio of 0.3, transverse crack rotor show downward trend in the $3x$ amplitude. The slant crack rotor on the contrary deviates somewhat from the steep upward trend for both vertical and horizontal directions. Hence, amplitude of $3x$ frequency component at 1/3rd critical speed is not a reliable way to diagnose the transverse crack without monitoring from early stage as the absence of $3x$ frequency component at this speed in general cannot be assumed to indicate the absence of a crack for rotor with transverse crack. The spectrum cascade for deeper transverse crack has also shown a very low $3x$ frequency component.

The $1x$ and $3x$ vibration response at 1/3rd critical speed show another important feature. The vertical vibration response is stronger than the horizontal for the $1x$ frequency component, whereas, for the $3x$ frequency component, the horizontal vibration response is stronger than the vertical. These are very crack-specific features as they are related to the stiffness variation due to breathing of crack. These features could be utilized in the monitoring and diagnosis of cracks in rotors. The effect of unbalance orientation angle relative to crack direction is also investigated and it has been found that only $1x$ frequency amplitude is affected and $2x$ and $3x$ frequency remain unaffected by unbalance phase. Hence, the trend of $3x$ frequency component can be used to detect the presence of propagating fatigue crack as well as identify the type of crack (transverse or slant). The spectrum cascade plot shown for transverse and slant cracks for different crack depths shows various subharmonic resonances, which are vital indicators of the presence of the crack. The nonlinear response-dependent breathing crack model helps better understand the dynamics of transverse- and slant-cracked rotor and reveals some of the hitherto unexplored response features.

Appendix A

For transverse crack, $\theta = 90^\circ$ and Eq. (9) reduce to

$$g_{11} = \frac{1}{E^1\pi R^4}\iint 2\alpha F_1^2\,\mathrm{d}A, \quad g_{22} = \frac{1}{E^1\pi R^4}\iint 2m_s k^2\alpha F_{\mathrm{III}}^2\,\mathrm{d}A,$$

$$g_{33} = \frac{1}{E^1\pi R^4}\iint 2k^2\alpha F_{\mathrm{II}}^2\,\mathrm{d}A, \quad g_{44} = \frac{1}{E^1\pi R^8}\iint 32\chi_0^2\alpha F_1^2\,\mathrm{d}A,$$

$$g_{55} = \frac{1}{E^1\pi R^8}\iint 32(R^2-\chi_0^2)\alpha F_2^2\,\mathrm{d}A,$$

$$g_{66} = \frac{1}{E^1\pi R^8}\iint \left[8\chi_0^2\alpha F_{\mathrm{II}}^2 + 8m_s(R^2-\chi_0^2)\alpha F_{\mathrm{III}}^2\right]\mathrm{d}A, \quad g_{12} = 0,$$

$$g_{14}=\frac{1}{E^1\pi R^6}\iint 8\chi_0\alpha F_1^2\,\mathrm{d}A,\quad g_{15}=\frac{1}{E^1\pi R^6}\iint 8\alpha F_1F_2\sqrt{(R^2-\chi_0^2)}\,\mathrm{d}A,$$

$$g_{16}=0,\quad g_{24}=0,\quad g_{25}=0,\quad g_{26}=\frac{1}{E^1\pi R^6}\iint 4m_sk\sqrt{(R^2-\chi_0^2)}\alpha F_{\mathrm{III}}^2\,\mathrm{d}A,$$

$$g_{36}=\frac{1}{E^1\pi R^6}\iint 4\chi_0k\alpha F_{\mathrm{II}}^2\,\mathrm{d}A,\quad g_{45}=\frac{1}{E^1\pi R^8}\iint 32\chi_0\alpha F_1F_2\sqrt{(R^2-\chi_0^2)}\,\mathrm{d}A,$$

$$g_{46}=0,\quad g_{56}=0. \tag{A.1}$$

For a shaft subjected to twisting moment excitation, the most probable orientation for a slant crack is $\theta=45^\circ$ and the orientation is of practical significance. For $\theta=45^\circ$, the flexibility expressions given in Eq. (9) reduce to

$$g_{11}=\frac{1}{E^1\pi R^4}\iint\left[\frac{\alpha}{2}F_1^2+\frac{m_s}{2}\alpha F_{\mathrm{III}}^2\right]\mathrm{d}A,\quad g_{22}=\frac{1}{E^1\pi R^4}\iint\left[2k^2\alpha F_1^2\right]\mathrm{d}A,$$

$$g_{33}=\frac{1}{E^1\pi R^4}\iint\left[k^2\alpha F_{\mathrm{II}}^2\right]\mathrm{d}A,\quad g_{44}=\frac{1}{E^1\pi R^8}\iint\left[4\chi_0^2\alpha F_1^2+4m_s\chi_0^2\alpha F_{\mathrm{III}}^2\right]\mathrm{d}A,$$

$$g_{55}=\frac{1}{E^1\pi R^8}\iint\left[4(2R^2-\chi_0^2)\alpha F_2^2+4m_s(2R^2-\chi_0^2)\alpha F_{\mathrm{III}}^2\right]\mathrm{d}A,$$

$$g_{66}=\frac{1}{E^1\pi R^8}\iint\left[4(2R^2-\chi_0^2)\alpha F_2^2+2\chi_0^2\alpha F_{\mathrm{II}}^2\right]\mathrm{d}A,$$

$$g_{12}=\frac{1}{E^1\pi R^4}\iint\left[k\alpha F_1^2\right]\mathrm{d}A,$$

$$g_{15}=\frac{1}{E^1\pi R^6}\iint\left[\sqrt{2}\alpha F_1F_2\sqrt{(2R^2-\chi_0^2)}+\sqrt{2}m_s\sqrt{(2R^2-\chi_0^2)}\alpha F_{\mathrm{III}}^2\right]\mathrm{d}A,$$

$$g_{16}=\frac{1}{E^1\pi R^6}\iint\left[\sqrt{2}\alpha F_1F_2\sqrt{(2R^2-\chi_0^2)}\right]\mathrm{d}A,\quad g_{24}=\frac{1}{E^1\pi R^6}\iint\left[2\sqrt{2}k\chi_0\alpha F_1^2\right]\mathrm{d}A,$$

$$g_{25}=\frac{1}{E^1\pi R^6}\iint\left[2\sqrt{2}k\alpha F_1F_2\sqrt{(2R^2-\chi_0^2)}\right]\mathrm{d}A,$$

$$g_{26}=\frac{1}{E^1\pi R^6}\iint\left[2\sqrt{2}k\alpha F_1F_2\sqrt{(2R^2-\chi_0^2)}\right]\mathrm{d}A,$$

$$g_{36}=\frac{1}{E^1\pi R^6}\iint\left[\sqrt{2}k\chi_0\alpha F_{\mathrm{II}}^2\right]\mathrm{d}A,$$

$$g_{45}=\frac{1}{E^1\pi R^8}\iint\left[4\chi_0\alpha F_1F_2\sqrt{(2R^2-\chi_0^2)}+4m_s\alpha\chi\sqrt{(2R^2-\chi_0^2)}\right]\mathrm{d}A,$$

$$g_{46}=\frac{1}{E^1\pi R^8}\iint\left[4\chi_0\alpha F_1F_2\sqrt{(2R^2-\chi_0^2)}\right]\mathrm{d}A,$$

$$g_{56}=\frac{1}{E^1\pi R^8}\iint\left[4\alpha F_2^2(2R^2-\chi_0^2)\right]\mathrm{d}A. \tag{A.2}$$

For the slant crack with $\theta = 45^\circ$, using $\bar{\alpha} = \alpha/R$, $\bar{h} = \alpha/h$, $\bar{\chi}_0 = \chi_0/\sqrt{2}R$, $\bar{a} = a/R$ and $\bar{b} = b/\sqrt{2}R$ the above flexibility coefficients can be expressed in non-dimensional form as

$$g_{11} = \frac{1}{\pi ER}\iint \frac{\bar{a}}{\sqrt{2}}(F_1^2 + m_s F_{III}^2)\,d\bar{\chi}_0\,d\bar{y}, \quad g_{12} = \frac{1}{\pi ER}\iint \sqrt{2}k\bar{a}F_1^2\,d\bar{\chi}_0\,d\bar{y},$$

$$g_{14} = \frac{1}{\pi ER}\iint 2\sqrt{2}\bar{\chi}_0\bar{a}(F_1^2 + m_s F_{III}^2)\,d\bar{\chi}_0\,d\bar{y},$$

$$g_{15} = \frac{1}{\pi ER^2}\iint 2\sqrt{2}\sqrt{1-\bar{\chi}_0^2}\bar{a}(F_1F_2 + m_s F_{III}^2)\,d\bar{\chi}_0 d\bar{y},$$

$$g_{16} = \frac{1}{\pi ER^2}\iint 2\sqrt{2}\sqrt{1-\bar{\chi}_0^2}\bar{a}F_1F_2\,d\bar{\chi}_0\,d\bar{y},$$

$$g_{22} = \frac{1}{\pi ER}\iint 2\sqrt{2}\bar{a}k^2F_1^2\,d\bar{\chi}_0\,d\bar{y},$$

$$g_{24} = \frac{1}{\pi ER^2}\iint 4\sqrt{2}k\bar{\chi}_0\bar{a}F_1^2\,d\bar{\chi}_0\,d\bar{y},$$

$$g_{25} = \frac{1}{\pi ER^2}\iint 4\sqrt{2}k\bar{a}\sqrt{1-\bar{\chi}_0^2}F_1F_2\,d\bar{\chi}_0\,d\bar{y},$$

$$g_{26} = \frac{1}{\pi ER^2}\iint 4\sqrt{2}k\bar{a}\sqrt{1-\bar{\chi}_0^2}F_1F_2\,d\bar{\chi}_0\,d\bar{y},$$

$$g_{33} = \frac{1}{\pi ER^2}\iint \sqrt{2}k^2\bar{a}F_{II}^2\,d\bar{\chi}_0 d\bar{y},$$

$$g_{36} = \frac{1}{\pi ER^2}\iint 2\sqrt{2}k\bar{\chi}_0\bar{a}F_{II}^2\,d\bar{\chi}_0\,d\bar{y},$$

$$g_{44} = \frac{1}{\pi ER^3}\iint (8\sqrt{2}\bar{\chi}_0^2\bar{a}F_I^2 + 8\sqrt{2}m_s\bar{\chi}_0^2\bar{a}F_{III}^2)\,d\bar{\chi}_0\,d\bar{y},$$

$$g_{45} = \frac{1}{\pi ER^3}\iint 8\sqrt{2}\bar{\chi}_0\bar{a}\sqrt{1-\bar{\chi}_0^2}(F_1F_2 + m_s F_{III}^2)\,d\bar{\chi}_0\,d\bar{y},$$

$$g_{46} = \frac{1}{\pi ER^3}\iint 8\sqrt{2}\bar{\chi}_0\bar{a}\sqrt{1-\bar{\chi}_0^2}F_1F_2\,d\bar{\chi}_0\,d\bar{y},$$

$$g_{55} = \frac{1}{\pi ER^3}\iint 8\sqrt{2}\bar{a}(1-\bar{\chi}_0^2)(F_2^2 + m_s F_{III}^2)\,d\bar{\chi}_0\,d\bar{y},$$

$$g_{56} = \frac{1}{\pi ER^3}\iint 8\sqrt{2}\bar{a}(1-\bar{\chi}_0^2)F_2^2\,d\bar{\chi}_0\,d\bar{y},$$

$$g_{66} = \frac{1}{\pi ER^3}\iint (8\sqrt{2}\bar{a}(1-\bar{\chi}_0^2)F_2^2 + 4\sqrt{2}\bar{\chi}_0^2\bar{a}F_{II}^2)\,d\bar{\chi}_0 d\bar{y}. \tag{A.3}$$

References

[1] J. Wauer, On the dynamics of cracked rotors—a literature survey, *Applied Mechanics Reviews* 43 (1990) 13–17.
[2] A.D. Dimarogonas, Vibration of cracked structures: a state of the art review, *Engineering Fracture Mechanics* 55 (1996) 831–857.
[3] G. Sabnavis, R.G. Kirk, M. Kasarda, D. Quinn, Cracked shaft detection and diagnostics: a literature review, *The Shock and Vibration Digest* 36 (2004) 287–296.

[4] K. Gupta, Rotor crack detection strategies—a review. *National Symposium on Rotor Dynamics (NSRD-2003)*, December 15–17, 2003, IIT, Guwahati, India.
[5] D.E. Bently, Vibration analysis techniques for detecting and diagnosing shaft cracks, *Orbit* (1986) 18–21.
[6] D. Bently, M. Werner, Extending machinery life, *Orbit* (1990) 5–9.
[7] I. Imam, S.H. Azzaro, R.J. Bankert, J. Scheibel, Development of an on-line rotor crack detection and monitoring system, *Journal of Vibration, Acoustics, Stress and Reliability in Design* 111 (1989) 241–250.
[8] R.A. Gasch, Survey of the dynamic behavior of a simple rotating shaft with a transverse crack, *Journal of Sound and Vibration* 160 (1993) 313–332.
[9] O.S. Jun, H.J. Eun, Y.Y. Earmme, C.W. Lee, Modeling and vibration analysis of a simple rotor with a breathing crack, *Journal of Sound and Vibration* 155 (1992) 273–290.
[10] C.A. Papadopoulos, A.D. Dimarogonas, Coupled vibration of cracked shafts, *Journal of Vibration and Acoustics* 114 (1992) 461–467.
[11] K.R. Collins, R.H. Plaut, J. Wauer, Detection of cracks in rotating Timoshenko shafts using axial impulses, *Journal of Vibration and Acoustics* 113 (1991) 74–78.
[12] A.K. Darpe, A. Chawla, K. Gupta, Analysis of the response of a cracked Jeffcott rotor to axial excitation, *Journal of Sound and Vibration* 249 (2002) 429–445.
[13] A.K. Darpe, K. Gupta, A. Chawla, Experimental investigations of the response of a cracked rotor to axial excitation, *Journal of Sound and Vibration* 260 (2003) 265–286.
[14] A.K. Darpe, K. Gupta, A. Chawla, Coupled bending, longitudinal and torsional vibrations of a cracked rotor, *Journal of Sound and Vibration* 269 (2004) 33–60.
[15] C.A. Papadopoulos, A.D. Dimarogonas, Coupled longitudinal and bending vibrations of a rotating shaft with an open crack, *Journal of Sound and Vibration* 117 (1987) 81–93.
[16] G.D. Gounaris, C.A. Papadopoulos, Crack identification in rotating shafts by coupled response measurements, *Engineering Fracture Mechanics* 69 (2002) 339–352.
[17] J.J. Sinou, A.W. Lees, The influence of cracks in rotating shafts, *Journal of Sound and Vibration* 285 (2005) 1015–1037.
[18] Y.P. Pu, J. Chen, J. Zou, P. Zhong, Quasi-periodic vibration of cracked rotor on flexible bearings, *Journal of Sound and Vibration* 251 (2002) 875–890.
[19] A.S. Sekhar, Identification of a crack in a rotor system using a model-based wavelet approach, *Structural Health Monitoring* 2 (2003) 293–308.
[20] A.S. Sekhar, Crack identification in a rotor system: a model-based approach, *Journal of Sound and Vibration* 270 (2004) 887–902.
[21] M.I. Friswell, J.E.T.P. Penny, Crack modelling for structural health monitoring, *International Journal of Structural Health Monitoring* 1 (2002) 139–148.
[22] N. Pugno, C. Surace, R. Ruotolo, Evaluation of the non-linear dynamic response to harmonic excitation of a beam with several breathing cracks, *Journal of Sound and Vibration* 235 (2000) 749–762.
[23] A.K. Darpe, K. Gupta, A. Chawla, Dynamics of a two-crack rotor, *Journal of Sound and Vibration* 259 (2003) 649–675.
[24] S.A. Adewusi, B.O. Al-Bedoor, Wavelet analysis of vibration signals of an overhang rotor with a propagating transverse crack, *Journal of Sound and Vibration* 246 (2001) 777–793.
[25] J. Zou, A. Chen, Comparative study on time–frequency feature of cracked rotor by Wigner–Ville distribution and wavelet transform, *Journal of Sound and Vibration* 276 (2004) 1–11.
[26] F. Wan, Q. Xu, S. Li, Vibration analysis of cracked rotor sliding bearing system with rotor–stator rubbing by harmonic wavelet transform, *Journal of Sound and Vibration* 271 (2004) 507–518.
[27] J. Zou, J. Chen, Y.P. Pu, Wavelet time–frequency analysis of torsional vibrations in rotor system with a transverse crack, *Computers & Structures* 82 (2004) 1181–1187.
[28] S. Prabhakar, A.S. Sekhar, A.R. Mohanty, Detection and monitoring of crack in a coast-down rotor supported on fluid film bearings, *Mechanical Systems and Signal Processing* 15 (2001) 447–450.
[29] T. Zhou, J. Xu, Z. Sun, Dynamic analysis and diagnosis of a cracked rotor, *Journal of Vibration and Acoustics* 123 (2001) 539–543.
[30] N. Bachschmid, P. Pennacchi, E. Tanzi, P. Verrier, F. Hasnaoui, K. Aabadi, Crack detectability in vertical axis cooling pumps during operation, *International Journal of Rotating Machinery* 10 (2004) 121–133.
[31] C. Zhu, D.A. Robb, D.J. Ewins, The dynamics of a cracked rotor with an active magnetic bearing, *Journal of Sound and Vibration* 265 (2003) 469–487.
[32] S.C. Huang, Y.M. Huang, S.M. Shieh, Vibration and stability of a rotating shaft containing a transverse crack, *Journal of Sound and Vibration* 162 (1993) 387–401.
[33] M.C. Wu, S.C. Huang, Vibration and crack detection of a rotor with speed-dependent bearings, *International Journal of Mechanical Science* 40 (1998) 545–555.
[34] M.C. Wu, S.C. Huang, In-plane vibration and crack detection of a rotating shaft-disk containing a transverse crack, *Journal of Vibration and Acoustics* 120 (1998) 551–556.
[35] G. Meng, R. Gasch, Stability and stability degree of a cracked flexible rotor supported on journal bearings, *Trans ASME, Journal of Vibration and Acoustics* 122 (2002) 116–125.
[36] M. Ichimonji, S. Watanabe, The dynamics of a rotor system with a shaft having a slant crack, *JSME International Journal Series III* 31 (1988).
[37] M. Ichimonji, S. Watanabe, Y. Kazao, S. Nonaka, The dynamic of a rotor system with a slant crack under torsional vibration, *Proceedings of the International Mechanical Engineering Congress & Exposition, ASME, Illinois* 192 (1994) 81–89.

[38] A.S. Sekhar, P. Balaji Prasad, Dynamic analysis of a rotor system considering a slant crack in the shaft, *Journal of Sound and Vibration* 208 (1997) 457–474.
[39] S. Prabhakar, A.S. Sekhar, A.R. Mohanty, Transient lateral analysis of a slant cracked rotor passing through its flexural critical speed, *Mechanism and Machine Theory* 37 (2002) 1007–1020.
[40] A.S. Sekhar, A.R. Mohanty, S. Prabhakar, Vibrations of cracked rotor system: transverse crack versus slant crack, *Journal of Sound and Vibration* 279 (2005) 1203–1217.